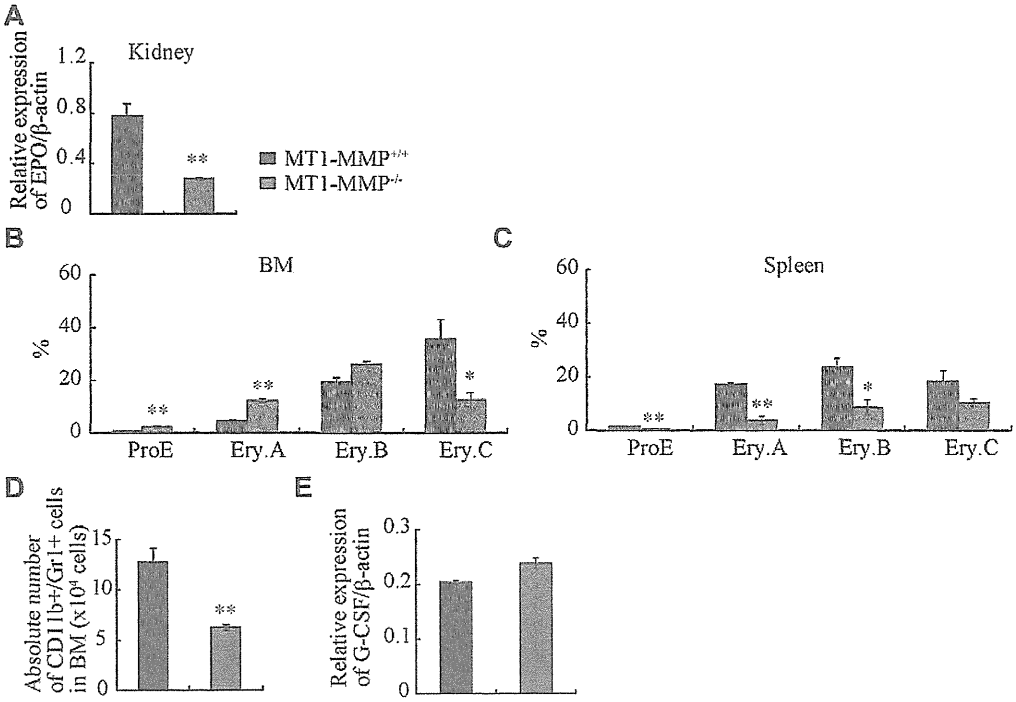

Figure 3. Erythroid and myeloid differentiation block in MT1-MMP$^{-/-}$ mice. (A) Real-time PCR of *Epo* in kidney (n = 3). (B-C) Percentage of different erythroblast populations during erythroid development (proE-EryA-EryB-EryC) of (B) BM cells or of (C) dissociated mouse spleen cells from MT1-MMP$^{+/+}$ (n = 5) and MT1-MMP$^{-/-}$ mice (n = 3). (D) Percentage of CD11b$^+$/Gr-1$^+$ cells per femur as determined by FACS (n = 5). Errors in bar graphs are SEM; **$P < .01$. (E) Real-time PCR of *G-CSF* in BM cells (n = 3).

The earliest T-cell progenitors are produced in the BM. We found an increase in the percentage of immature CD4$^-$CD8$^-$c-Kit$^-$CD44$^-$ cells T cells in MT1-MMP$^{-/-}$ BM cells ($4.1 \times 10^5 \pm 0.2 \times 10^5$ cells in MT1-MMP$^{-/-}$ and $2.6 \times 10^5 \pm 0.3 \times 10^5$ cells in MT1-MMP$^{+/+}$ BM, respectively; n = 4, $P < .05$). The MT1-MMP$^{-/-}$ thymus (Figure 2G) was small with a low number of thymocytes (Figure 2H). Thymic lobes, and specifically the medullar region, appeared smaller than in MT1-MMP$^{+/+}$ mice (Figure 2I). Flow cytometric analysis of thymocytes revealed no difference in the percentage of immature CD4$^-$ or CD8$^-$ double-negative (DN) thymocytes or of CD4$^-$CD8$^-$c-Kit$^-$CD44$^-$ thymocytes between the MT1-MMP$^{+/+}$ and the MT1-MMP$^{-/-}$ mice. However, a relative decrease in the percentage of the more mature CD4$^+$CD8$^+$ double-positive (DP) thymocyte population and in the CD4$^+$ single-positive (SP) cell population was revealed in thymocytes from the MT1-MMP$^{-/-}$ mice (Figure 2J). In absolute terms, CD4 SP numbers were reduced 2.5-fold, CD8 SP 2.1-fold, and DP thymocytes 5.3-fold, whereas the DN population remained unaffected. These data indicate that T-cell progenitors developed within the BM even in the absence of MT1-MMP, but that their further differentiation in the thymus was blocked at or before development of the immature DN thymocyte population, causing default differentiation into CD4 cell SP and NK-cell lineages.

To assess whether the abnormal thymic colonization observed in MT1-MMP$^{-/-}$ mice was because of the loss of MT1-MMP in hematopoietic cells or in stromal cells, MT1-MMP$^{+/+}$ and MT1-MMP$^{-/-}$ BM donor cells were transplanted into lethally irradiated wild-type recipients. Chimeras were analyzed 4 months after transplantation. T- and B-cell differentiation of transplanted MT1-MMP$^{-/-}$ cells (expressing the Ag Ly5.2 (CD45.2) on leukocytes) within the BM were normal (Figure 2K-L). These data indicated that MT1-MMP$^{-/-}$ mice showed impaired T- and B-cell development. Even though MT1-MMP$^{-/-}$ mice showed a hematopoietic cell defect (see Figure 1), MT1-MMP$^{-/-}$ BM cells retained the potential to differentiate into T- and B-cell lineages in an MT1-MMP$^{+/+}$ environment. These data indicate that, aside from its influence on stem cells, MT1-MMP also plays an additional role in regulating the BM niche.

MT1-MMP ablation impairs erythroid and myeloid differentiation

Anemia, as seen in 14-day-old MT1-MMP mice (see Figure 1C), is expected to trigger a compensatory response that is mediated principally through increased serum levels of erythropoietin (*Epo*), a master cytokine of erythropoiesis. Epo controls growth, survival, and differentiation of erythroid progenitors, either cooperatively with, or independently of KitL.[32-34] Despite severe anemia, *Epo* mRNA expression in kidney tissues of MT1-MMP$^{-/-}$ mice was low (Figure 3A) and the expected compensatory increase in spleen size did not occur (see Figure 2B).

To assess erythroid differentiation, we examined CD71 and TER119 expression in the BM and splenic erythroblasts, and classified erythroid cells into 4 populations at progressive levels of differentiation: proerythroblasts TER119^{med}CD71^{high}FSC^{high} (ProE), TER119^{high}CD71^{high}FSC^{high} (Ery.A), TER119^{high}CD71^{high}FSC^{low} (Ery.B), and TER119^{high}CD71^{low}FSC^{low} (Ery.C).[35]

MT1-MMP$^{-/-}$ BM erythroid lineage cells accumulated at the ProE, Ery.A, and Ery.B stage, and cells at the late erythroblast differentiation stages (Ery.C) were reduced (Figure 3B). In spleen, all stages of erythroid lineage cells were reduced in MT1-MMP$^{-/-}$ mice (Figure 3C). These data suggest that MT1-MMP is involved in both BM and splenic erythropoiesis, and that the defect in erythropoiesis in MT1-MMP$^{-/-}$ mice might be due, in part, to impaired Epo production.

Granulocytic cells of adult mouse BM express CD11b and high amounts of Gr-1. The absolute number of CD11b$^+$/Gr-1$^+$ granulocytes was lower in MT1-MMP$^{-/-}$ than in MT1-MMP$^{+/+}$ BM cells (Figure 3D). G-CSF is a growth, differentiation, and activating factor for neutrophils and their precursors. Regardless of the observed neutropenia, no difference in *G-CSF* (Figure 3E) or thrombopoietin (*Tpo*; data not shown) expression was observed in the BM cells of these mice, indicating that other factors might be responsible for the impaired myelopoiesis.

MT1-MMP deficiency reduces stromal cell–derived cytokine production

Chimera experiments indicated that the observed hematopoietic defect in MT1-MMP–deficient mice was in part because of a niche defect, suggesting that dysregulated production of stromal cell–derived cytokine(s) may be responsible for the hematopoietic differentiation block observed in MT1-MMP$^{-/-}$ mice. BM and thymic stromal cells produce IL-7.[36] Plasma levels of the stromal cell–derived factors KitL, SDF-1α, and IL-7 were lower in MT1-MMP$^{-/-}$ mice than in MT1-MMP$^{+/+}$ mice (Figure 4A-C). We observed a reduced number of nestin$^+$ niche cells in MT1-MMP$^{-/-}$ mice and, interestingly, nestin$^+$ niche cells highly express KitL and SDF-1.[31] In accordance with these data, MT1-MMP$^{-/-}$ BM cells and MT1-MMP$^{-/-}$ primary stromal cells showed lower mRNA expression of *IL-7, KitL*, and *SDF-1α/CXCL12* compared with MT1-MMP$^{+/+}$ cells (Figure 4D, supplemental Figure 1). In addition, very few primary stromal cells grew in cultures established using MT1-MMP$^{-/-}$ BM cells (supplemental Figure 1).

To exclude the possibility that the growth/chemokine factor decrease in MT1-MMP$^{-/-}$ mice was because of a lower number of the growth factor–producing stromal cells, we modulated MT1-MMP expression on a murine stromal cell line (MS-5). Overexpression of MT1-MMP in MS-5 stromal cells (MT1-MMP TF) increased *KitL, SDF-1α*, and *IL-7* gene expression (Figure 4E). In contrast, MT1-MMP knock down in MS-5 murine stromal cells using shRNA (*MT1-MMP KD*) reduced the expression of *KitL, SDF-1α*, and *IL-7* mRNA than control MS-5 cells (Figure 4F). Consistent with this result, less KitL, SDF-1α, and IL-7 protein was detected in supernatants of MT1-MMP KD cultures compared with control cultures as determined by ELISA (Figure 4G). The frequency of CXCR4 (the SDF-1 receptor) and c-Kit (the KitL receptor) expressing Sca-1$^+$ MT1-MMP$^{-/-}$ BMMCs was not significantly changed (data not shown). These data indicate that loss of MT1-MMP activity in stromal cells reduced signaling by IL-7, KitL, and SDF-1α, factors known to regulate B and T lymphopoiesis and erythropoiesis.

We next examined the release and expression of these factors by primary *MEFs*. Confirming our BM cell and primary stromal cell cytokine/chemokine data, low expression of *KitL, SDF-1α*, and *IL-7* was found in MT1-MMP$^{-/-}$ MEFs (Figure 4H-I).

To investigate whether the observed impaired production of cytokines/chemokines would also result in impaired function, we set up an MEF feeder–based culture supplemented with IL-3. Whereas Lin$^-$ cells differentiated in MT1-MMP$^{+/+}$ MEF-supported cultures, the number of CD11b$^+$/Gr-1$^+$ cells in MT1-MMP$^{-/-}$ cultures did not change significantly (Figure 4J). Addition of neutralizing Abs against KitL confirmed that the observed myeloid cell differentiation was mainly because of the KitL that was released by the cultures.

We set up a migration assay to investigate SDF-1α function. Lin$^-$ cells derived from BM cells migrated toward an MT1-MMP$^{+/+}$ MEF supernatant, a process that is mediated by SDF-1, as shown by using neutralizing Abs against SDF-1. In contrast, no migration of Lin$^-$ cells was observed toward an MT1-MMP$^{-/-}$ supernatant (Figure 4K).

MT1-MMP increases cytokine/chemokine production in niche cells by suppressing HIF-1α

The *HIF* gene is known to regulate VEGF, placental growth factor, angiopoietin 2, platelet-derived growth factor-B, SDF-1α, Epo, and KitL/SCF expression.[7] HIF-1α activity under normoxia depends on the FIH-1. FIH1-mediated hydroxylation disrupts a critical interaction between HIFα and the coactivators p300/CBP, impairing HIF transcriptional activity.[37,38] To determine whether HIF signaling is involved in MT1-MMP modulation of hematopoietic differentiation, we assessed HIF-1α, HIF-2α, and FIH-1 protein levels in MT1-MMP knockdown and control MS-5 cells. MT1-MMP knockdown did not affect HIF-1α or HIF-2α protein expression (supplemental Figure 2), but did up-regulate FIH-1 protein expression within the cytosol of MS-5 cells (Figure 5A), where FIH-1 can prevent HIF-1α binding to the transcriptional coactivator p300/CBP thereby blocking HIF-1-induced transcription of genes such as SDF-1 and KitL.[39] Immunohistochemical analysis showed that less nestin$^+$ stromal cells coexpressing FIH-1 were found in MT1-MMP$^{-/-}$ BM cells than in MT1-MMP$^{+/+}$ BM cells (Figure 5B). These findings are consistent with previous data that, in monocytes, the cytoplasmic tail of MT1-MMP binds to FIH-1, leading to inhibition of FIH-1 activity by its inhibitor, Mint3/APBA3.[23]

HIF-1 immunostaining showed that HIF-1, in contrast to its expression in MT1-MMP$^{+/+}$ BM cells, was preferentially expressed in the cytoplasm of MT1-MMP$^{-/-}$ BM cells (Figure 5C).

Our data suggested that MT1-MMP can activate the HIF1 pathway in stromal cells as it does in monocytes. We therefore hypothesized that FIH-1 overexpression in stromal cells would cause a reduction in cytokine/chemokine production, which was indeed the case (Figure 5D-F). These data suggested that FIH-1 overexpression reduced SDF-1, KitL, and IL-7 gene transcription in stromal cells. Furthermore, although the knockdown efficiency of FIH-1 by shRNA was only 30%, FIH-1 knockdown rescued *KitL, SDF-1α*, and *IL-7* gene expression in MT1-MMP knockdown (70% reduction by siRNA) MS-5 cells (Figure 5G-I) indicating that the decreased HIF-mediated cytokine gene transcription in MT1-MMP knockdown stromal cells can be partially rescued by blocking FIH-1 activity. These data highlight the importance of MT1-MMP–mediated HIF-1 activation for the transcriptional regulation of critical hematopoietic niche factors.

Exogenous SDF-1α and KitL addition restores leukopenia and thrombopenia in MT1-MMP$^{-/-}$ mice

Finally, we asked whether growth factor addition would rescue the observed block in leukopenia and thrombopenia because of MT1-MMP deficiency. Indeed, addition of recombinant IL-7 to MT1-MMP$^{-/-}$ or wild-type BMMC cultures induced a similar number of B-cell colonies (CFU–IL-7) in the MT1-MMP$^{-/-}$ as in the wild-type cells (Figure 6A).

MS-5 cells support myeloid cell differentiation of Lin$^-$ wild-type cells in vitro. However, fewer GFP$^+$ hematopoietic cells were generated from Lin$^-$ wild-type BM cells on MT1-MMP KD MS-5 stromal cells than on control MS-5 cells. Addition of KitL restored hematopoietic cell growth on the MT1-MMP KD MS-5 feeder cultures (Figure 6B).

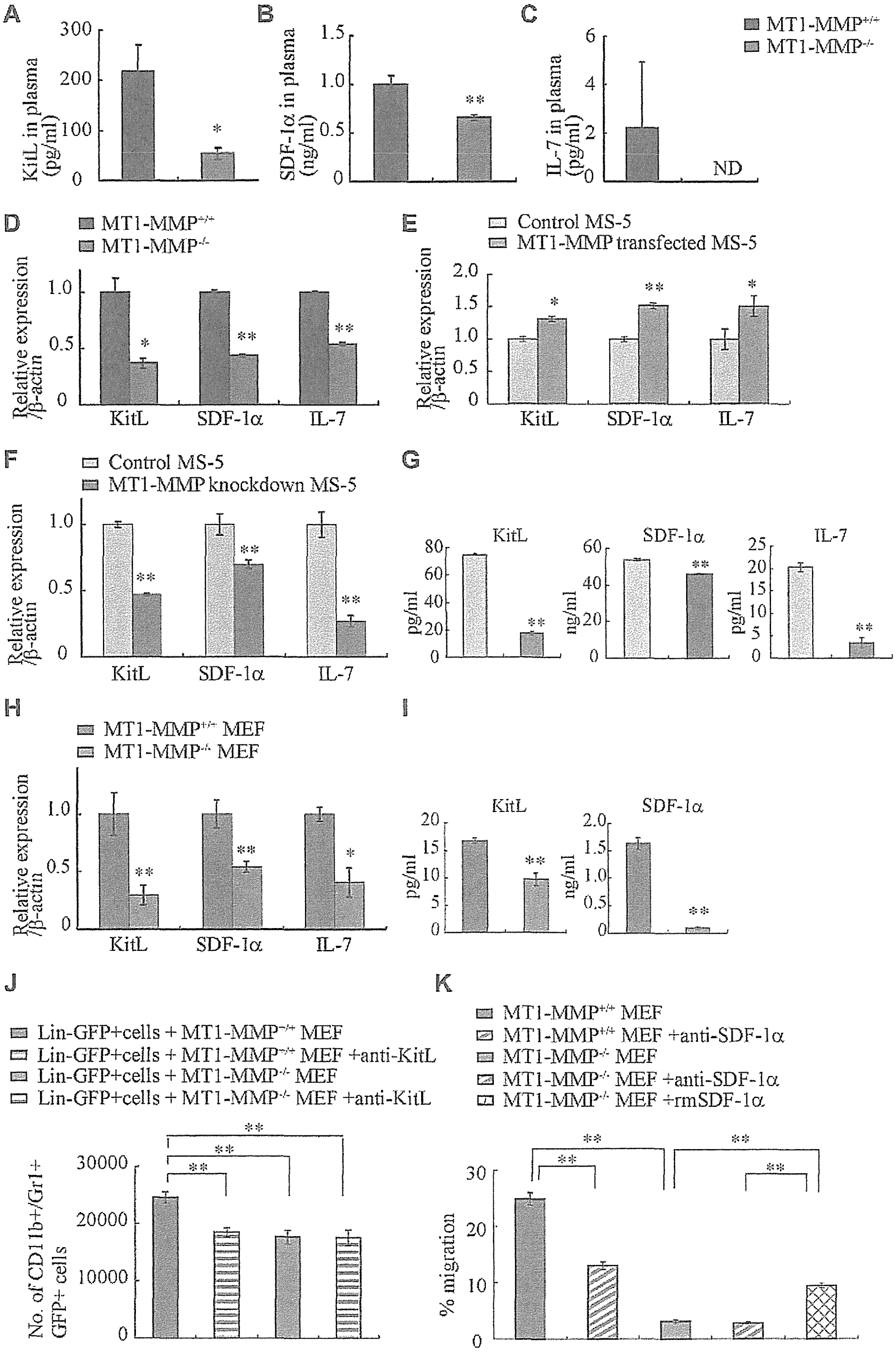

Figure 4. MT1-MMP deficiency prevents transcription of niche chemokines/cytokines. (A-C) KitL, SDF-1α, and IL-7 plasma levels in MT1-MMP$^{+/+}$ and MT1-MMP$^{-/-}$ plasma were measured by ELISA (n > 6). *KitL*, *SDF-1α*, and *IL-7* gene expression in (D) total BM cells, (E) MS-5 control and MT1-MMP–overexpressing cells, and (F) MT1-MMP knockdown (KD) and control MS-5 cells were analyzed using real-time PCR. The results are expressed relative to expression of a *β-actin*. (G) KitL, SDF-1α, and IL-7 protein levels in MT1-MMP knockdown (KD) and control MS-5 cell-culture supernatants were determined by ELISA. (H) *KitL*, *SDF-1α*, and *IL-7* gene expression in MT1-MMP$^{+/+}$ and MT1-MMP$^{-/-}$ MEF cells was determined using real-time PCR. The results are expressed relative to expression of *β-actin*. (I) KitL and SDF-1α protein levels in the indicated MEF cell-culture supernatants were evaluated by ELISA. (J) Lin$^-$GFP$^+$ cells were cultured on MT1-MMP$^{+/+}$ and MT1-MMP$^{-/-}$ MEF cells in the presence or absence of neutralizing Abs against KitL. The number of CD11b$^+$Gr1$^+$ cells was assessed after 7 days by FACS (n = 5). (K) Lin$^-$ cells were plated in transwells. MT1-MMP$^{+/+}$ and MT1-MMP$^{-/-}$ MEF cell-culture supernatants supplemented with recombinant SDF-1α were added to the lower chamber. Neutralizing Abs against SDF-1α were added to both chambers. The percentage of migrated cells was determined (n = 9 from 2 independent experiments). Errors in bar graphs are SEM; *$P < .05$, **$P < .01$. Data shown are representative of 3 to 4 independent experiments.

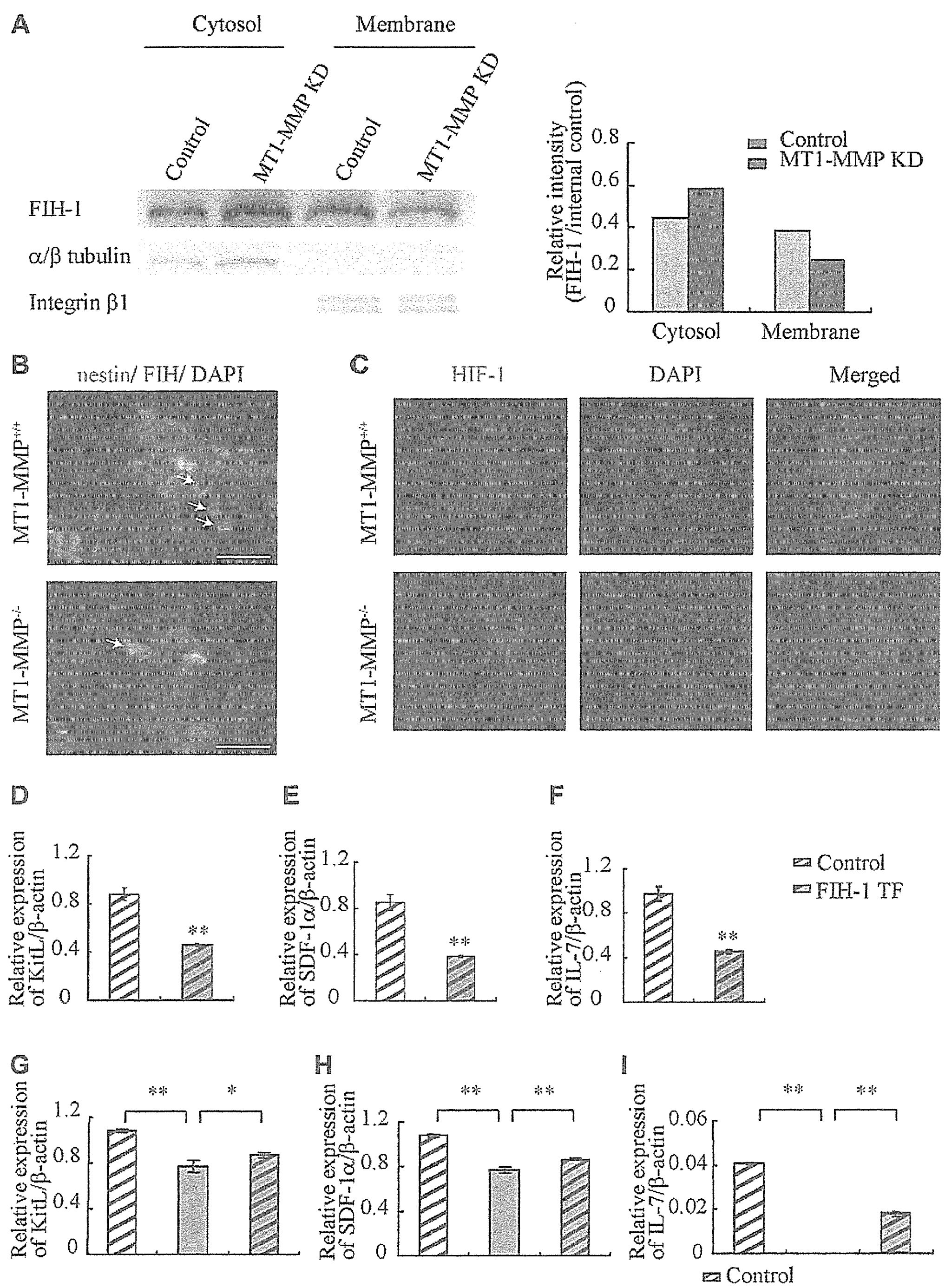

Figure 5. MT1-MMP deficiency prevents HIF-mediated transcription of niche factors. (A) FIH-1 expression in subcellular fractions was analyzed by Western blotting. α/β tubulin and integrin-β1 are representative cytosolic and membrane proteins, respectively. (B) Representative images of immunofluorescent staining of nestin (green fluorescence) and FIH-1 (red fluorescence) in BM sections derived from MT1-MMP$^{+/+}$ and MT1-MMP$^{-/-}$ mice. The arrows indicate nestin^{+}/FIH-1 cells. Nuclei were counterstained with DAPI (blue; bars, 100 μm). (C) Representative images of immunofluorescent staining of HIF-1α (green fluorescence) in BM cells derived from MT1-MMP$^{+/+}$ and MT1-MMP$^{-/-}$ mice. Nuclei were counterstained with DAPI (blue). (D-I) *KitL*, *SDF-1α* and *IL-7* gene expression in (D-F) MS-5 cells overexpressing FIH-1, and (G-I) in MT1-MMP–deficient MS-5 cells with or without *FIH-1* knockdown as analyzed using real-time PCR. The results are expressed relative to expression of a *β-actin*, which was set at 1.0. Data shown are representative of 3 to 4 independent experiments.

Similarly, KitL treatment restored WBC and PLT numbers in the PB in MT1-MMP$^{-/-}$ mice to the values of wild-type controls (Figure 6C-D) and a single injection of SDF-1α increased both WBC and PLT counts in the PB of MT1-MMP$^{-/-}$ mice 2 days after injection (Figure 6E-F). Although hematopoietic cell growth was restored in MT1-MMP$^{-/-}$ mice by injection of KitL or SDF-1, survival was not improved (data not shown).

Collectively, these results suggest that MT1-MMP alters the HSC niche by modulating HIF signaling, which promotes cytokine production and enhances cell differentiation and migration.

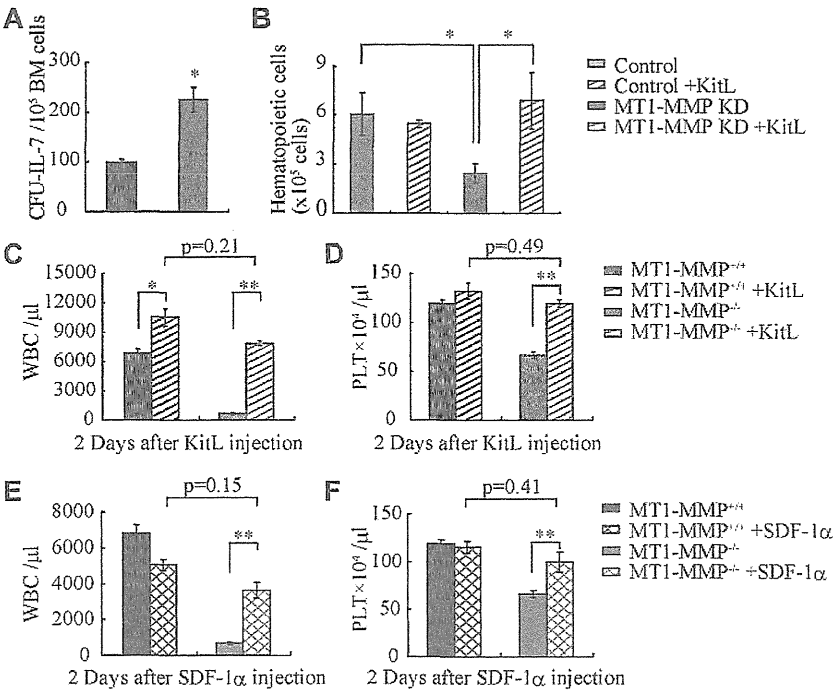

Figure 6. MT1-MMP–deficient mice have a defective BM stromal niche with impaired terminal differentiation because of impaired release of HIF-1α–associated factors. (A) Number of colonies in IL-7–containing cultures of MT1-MMP$^{+/+}$ and MT1-MMP$^{-/-}$ BM cells (n = 3). (B) Coculture of wild-type Lin$^-$ BM GFP$^+$ cells on *confluent MT1-MMP knockdown or control MS-5 cells* with/without KitL. (C-D) PB WBCs (C) and PLT (D) after KitL injections into MT1-MMP$^{+/+}$ (n ≥ 10) and MT1-MMP$^{-/-}$ mice (n = 3). (E-F) PB WBCs (E) and PLT (F) counts 2 days after initiation of SDF-1 treatment of MT1-MMP$^{+/+}$ (n ≥ 10) and MT1-MMP$^{-/-}$ mice (n = 2). Errors in bar graphs are SEM; $^*P < .05$, $^{**}P < .01$.

Discussion

In this report, we identified MT1-MMP as a key player of postnatal hematopoiesis. We demonstrate that MT1-MMP–expressing cells serve as key links between the HIF-1 regulatory system and transcriptional regulation of vital niche chemokines/cytokines necessary for HSC maintenance and cell differentiation (Figure 7). Specifically, we show that MT1-MMP deficiency leads to impairment of steady-state hematopoiesis because of a reduced HSC pool and a trilineage differentiation block. Mechanistically, we provide evidence that MT1-MMP deficiency in niche/stromal cells increases cytosolic FIH1 on expense of the membrane-associated FIH1 expression, thereby preventing transcription of the HIF-responsive genes EPO, KitL, IL-7, and SDF-1α. Thus, this study identifies MT1-MMP as a key molecular link between hypoxia and the regulation of vital HSC niche factors.

We reported that MMP-9 and plasminogen activation is important for the ectodomain shedding of the hematopoietic growth factor like KitL.[10,19] MT1-MMP can activate various proteases, including plasminogen or MMP-2, which in turn can activate MMP-9. It has been reported that MMP-2 activation can process

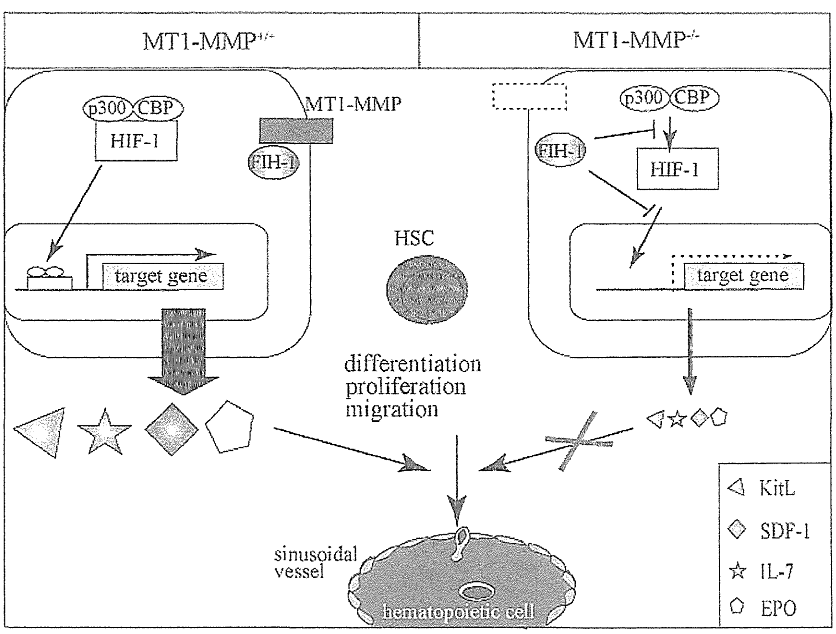

Figure 7. Proposed model of the role of MT1-MMP–expressing niche cells, which serve as key links between the HIF-1 regulatory system and transcriptional regulation of vital niche chemokines/cytokines necessary for HSC maintenance and cell differentiation. MT1-MMP deficiency in niche cells up-regulates FIH1 expression, thereby preventing transcription of the HIF-responsive genes *EPO*, *KitL*, *IL-7*, and *SDF-1α*. MT1-MMP deficiency leads to impaired steady-state hematopoiesis because of a trilineage differentiation block.

SDF-1/CXCL12.[40] We are currently examining whether ectodomain shedding by MT1-MMP–activated MMPs could be another reason for the low cytokine levels observed in MT1-MMP$^{-/-}$ mice.

Other known modulators of the BM and of niches such as the cancer stem cell niche, including vascular endothelial growth factor-A, angiopoietin 2, placental growth factor, and platelet-derived growth factor B, are also HIF-regulated target genes and therefore might also depend on MT1-MMP function.[7,8,41-43] But further studies will be needed to proof this concept.

Using BM chimeras generated using MT1-MMP$^{-/-}$ and MT1-MMP$^{+/+}$ donor cells, we showed that the developmental T-cell differentiation arrest observed in MT1-MMP$^{-/-}$ mice was mainly because of a niche defect, and not because of the impaired stem cell pool observed in these mice. In MT1-MMP$^{-/-}$ mice, we found preferential differentiation into CD4 SP thymocytes, which is most likely because of impaired Notch signaling.[44] Indeed, a recent study demonstrated that MT1-MMP directly cleaves Dll-1, a Notch ligand on BM stromal cells.[45] The continued presence of Dll-1 is required for T-cell commitment and maintenance at the DN1 and DN2 stages of thymocyte development. In the absence of Notch signaling, the developing DN1 and DN2 thymocytes adopt a NK-cell fate by default, a phenomena that we indeed observed in the MT1-MMP$^{-/-}$ mice.[46]

IL-7 signaling and Notch signaling are implicated in B-cell lymphopoiesis.[47] We found that HSC differentiation toward B lymphocytes was compromised in MT1-MMP–deficient BM cells. The long-term proliferation capacity of BM pre-B1 cells is known to be critically dependent on KitL and IL-7 expression and signaling, factors that we have shown require the presence of MT1-MMP for their expression.[48,49] Furthermore, we provide evidence that MT1-MMP deficiency in stromal cells also impairs the expression of SDF-1α, which is a key regulator of B-cell lymphopoiesis and BM myelopoiesis.[50] Our data are consistent with those of a previous report, which observed that defects in B lymphopoiesis are modulated by MT1-MMP–mediated cleavage of Dll-1 on BM stromal cells.[45] Impaired BM myelopoiesis was found in MT1-MMP–deficient mice, regardless of the fact that G-CSF expression was normal. Factors such as KitL and SDF-1α have also been implicated in myelopoiesis, and therefore might be at least partially responsible for the observed phenotype.

In addition, in vivo administration of KitL and SDF-1α rescued the pancytopenia in MT1-MMP–deficient mice. As both growth factors can increase the egress and mobilization of mature hematopoietic cells, but also can promote hematopoietic cell differentiation, the restoration of PB counts in MT1-MMP–deficient mice could be because of improved hematopoietic cell migration and/or differentiation. We confirmed data by Vagima et al demonstrating that MT1-MMP is expressed on hematopoietic progenitor cells.[21] This group showed that MT1-MMP is required for G-CSF–mediated hematopoietic progenitor cell mobilization.

SDF-1α is required for the maintenance of BM HSCs and is expressed by both perivascular and endosteal cells.[11,13] Deficits in the maintenance of the HSC pool in the absence of CXCR4 are HSC autonomous. Indeed, we could show that MT1-MMP deficiency altered SDF-1α/CXCL12-CXCR4 signaling and impaired the stem cell pool.

Our studies on the role of MT1-MMP in hematopoietic niche/stromal cells provide the rationale for further exploration of MT1-MMP in other hypoxic niches, for example, the cancer niche or the "ischemia-associated niche," as MT1-MMP seems to control the hematopoietic cell response in those diseases by controlling cytokine production.

Acknowledgments

The authors thank the FACS core facility in the Institute of Medical Science (University of Tokyo) for their help. They also thank Dr Hideo Ema for critical advice. Stephanie C. Napier kindly provided editorial assistance to the authors during the preparation of this manuscript. Pauline O'Grady edited the manuscript.

This work was supported by grants from the Japan Society for the Promotion of Science and Grants-in-Aid for Scientific Research from the Ministry of Education, Culture, Sports, Science and Technology (MEXT; K.H. and B.H.); a Grant-in-Aid for Scientific Research on Priority Areas from the MEXT (K.H.); the Mitsubishi Pharma Research Foundation (K.H.); a Grant-in-Aid for Scientific Research on Innovative Areas from the MEXT (B.H.); and the Program for Improvement of the Research Environment for Young Researchers (B.H.) funded by the Special Coordination Funds for Promoting Science and Technology of the MEXT, Japan. In addition, this work was supported by grants from ENSHIN Medical Research Foundation, from Kyowa Hakko Kirin Co Ltd, and from Daiichi Sankyo Company Ltd (K.H.).

Authorship

Contribution: C.N., B.H., and K.H. designed and performed experiments, analyzed and interpreted data, and wrote the manuscript; K.K., Y.T., I.G., A.S., M.O.-K., Y.M., M.N., T.S., N.K., T.K., and S.K.-K. participated in performing experiments, data analysis, and discussion; M.S. and H.N. interpreted data; and H.N., B.H., and K.H. assisted with experimental design and manuscript writing.

Conflict-of-interest disclosure: The authors declare no competing financial interests.

Correspondence: Koichi Hattori, MD, PhD, Center for Stem Cell Biology and Regenerative Medicine, Institute of Medical Science at the University of Tokyo, 4-6-1, Shirokanedai, Minato-ku, Tokyo 108-8639, Japan; e-mail: khattori@ims.u-tokyo.ac.jp.

References

1. Schofield R. The relationship between the spleen colony-forming cell and the haemopoietic stem cell. *Blood Cells.* 1978;4(1-2):7-25.
2. Adams GB, Chabner KT, Alley IR, et al. Stem cell engraftment at the endosteal niche is specified by the calcium-sensing receptor. *Nature.* 2006; 439(7076):599-603.
3. Takubo K, Goda N, Yamada W, et al. Regulation of the HIF-1alpha level is essential for hematopoietic stem cells. *Cell Stem Cell.* 2010;7(3):391-402.
4. Jang YY, Sharkis SJ. A low level of reactive oxygen species selects for primitive hematopoietic stem cells that may reside in the low-oxygenic niche. *Blood.* 2007;110(8):3056-3063.
5. Adelman DM, Maltepe E, Simon MC. Multilineage embryonic hematopoiesis requires hypoxic ARNT activity. *Genes Dev.* 1999;13(19):2478-2483.
6. Scortegagna M, Morris MA, Oktay Y, Bennett M, Garcia JA. The HIF family member EPAS1/HIF-2alpha is required for normal hematopoiesis in mice. *Blood.* 2003;102(5):1634-1640.
7. Rey S, Semenza GL. Hypoxia-inducible factor-1-dependent mechanisms of vascularization and vascular remodelling. *Cardiovasc Res.* 2010; 86(2):236-242.
8. Hattori K, Heissig B, Wu Y, et al. Placental growth factor reconstitutes hematopoiesis by recruiting VEGFR1(+) stem cells from bone-marrow microenvironment. *Nat Med.* 2002;8(8):841-849.
9. Arai F, Hirao A, Ohmura M, et al. Tie2/angiopoietin-1 signaling regulates hematopoietic stem cell quiescence in the bone marrow niche. *Cell.* 2004; 118(2):149-161.
10. Heissig B, Hattori K, Dias S, et al. Recruitment of stem and progenitor cells from the bone marrow

niche requires MMP-9 mediated release of kit-ligand. *Cell.* 2002;109(5):625-637.

11. Kollet O, Dar A, Shivtiel S, et al. Osteoclasts degrade endosteal components and promote mobilization of hematopoietic progenitor cells. *Nat Med.* 2006;12(6):657-664.
12. Ehninger A, Trumpp A. The bone marrow stem cell niche grows up: mesenchymal stem cells and macrophages move in. *J Exp Med.* 2011;208(3): 421-428.
13. Sugiyama T, Kohara H, Noda M, Nagasawa T. Maintenance of the hematopoietic stem cell pool by CXCL12-CXCR4 chemokine signaling in bone marrow stromal cell niches. *Immunity.* 2006; 25(6):977-988.
14. Tokoyoda K, Egawa T, Sugiyama T, Choi BI, Nagasawa T. Cellular niches controlling B lymphocyte behavior within bone marrow during development. *Immunity.* 2004;20(6):707-718.
15. Egawa T, Kawabata K, Kawamoto H, et al. The earliest stages of B cell development require a chemokine stromal cell-derived factor/pre-B cell growth-stimulating factor. *Immunity.* 2001;15(2): 323-334.
16. Fleming HE, Paige CJ. Pre-B cell receptor signaling mediates selective response to IL-7 at the pro-B to pre-B cell transition via an ERK/MAP kinase-dependent pathway. *Immunity.* 2001; 15(4):521-531.
17. Peschon JJ, Morrissey PJ, Grabstein KH, et al. Early lymphocyte expansion is severely impaired in interleukin 7 receptor-deficient mice. *J Exp Med.* 1994;180(5):1955-1960.
18. von Freeden-Jeffry U, Vieira P, Lucian LA, McNeil T, Burdach SE, Murray R. Lymphopenia in interleukin (IL)-7 gene-deleted mice identifies IL-7 as a nonredundant cytokine. *J Exp Med.* 1995; 181(4):1519-1526.
19. Heissig B, Lund LR, Akiyama H, et al. The plasminogen fibrinolytic pathway is required for hematopoietic regeneration. *Cell Stem Cell.* 2007; 1(6):658-670.
20. Lehti K, Rose NF, Valavaara S, Weiss SJ, Keski-Oja J. MT1-MMP promotes vascular smooth muscle dedifferentiation through LRP1 processing. *J Cell Sci.* 2009;122:126-135.
21. Vagima Y, Avigdor A, Goichberg P, et al. MT1-MMP and RECK are involved in human CD34+ progenitor cell retention, egress, and mobilization. *J Clin Invest.* 2009;119(3):492-503.
22. Chun TH, Hotary KB, Sabeh F, Saltiel AR, Allen ED, Weiss SJ. A pericellular collagenase directs the 3-dimensional development of white adipose tissue. *Cell.* 2006;125(3):577-591.
23. Sakamoto T, Seiki M. A membrane protease regulates energy production in macrophages by activating hypoxia-inducible factor-1 via a non-proteolytic mechanism. *J Biol Chem.* 2010; 285(39):29951-29964.
24. Sakamoto T, Seiki M. Cytoplasmic tail of MT1-MMP regulates macrophage motility independently from its protease activity. *Genes Cells.* 2009;14(5):617-626.
25. Itoh Y, Seiki M. MT1-MMP: a potent modifier of pericellular microenvironment. *J Cell Physiol.* 2006;206(1):1-8.
26. Hotary KB, Allen ED, Brooks PC, Datta NS, Long MW, Weiss SJ. Membrane type I matrix metalloproteinase usurps tumor growth control imposed by the three-dimensional extracellular matrix. *Cell.* 2003;114(1):33-45.
27. Seiki M. Membrane-type 1 matrix metalloproteinase: a key enzyme for tumor invasion. *Cancer Lett.* 2003;194(1):1-11.
28. Holmbeck K, Bianco P, Caterina J, et al. MT1-MMP-deficient mice develop dwarfism, osteopenia, arthritis, and connective tissue disease due to inadequate collagen turnover. *Cell.* 1999;99(1): 81-92.
29. Hattori K, Heissig B, Tashiro K, et al. Plasma elevation of stromal cell-derived factor-1 induces mobilization of mature and immature hematopoietic progenitor and stem cells. *Blood.* 2001; 97(11):3354-3360.
30. Taniwaki K, Fukamachi H, Komori K, et al. Stroma-derived matrix metalloproteinase (MMP)-2 promotes membrane type 1-MMP-dependent tumor growth in mice. *Cancer Res.* 2007;67(9):4311-4319.
31. Mendez-Ferrer S, Michurina TV, Ferraro F, et al. Mesenchymal and haematopoietic stem cells form a unique bone marrow niche. *Nature.* 2010; 466(7308):829-834.
32. Maiese K, Chong ZZ, Shang YC. Raves and risks for erythropoietin. *Cytokine Growth Factor Rev.* 2008;19(2):145-155.
33. Munugalavadla V, Kapur R. Role of c-Kit and erythropoietin receptor in erythropoiesis. *Crit Rev Oncol Hematol.* 2005;54(1):63-75.
34. Wang W, Horner DN, Chen WL, Zandstra PW, Audet J. Synergy between erythropoietin and stem cell factor during erythropoiesis can be quantitatively described without co-signaling effects. *Biotechnol Bioeng.* 2008;99(5):1261-1272.
35. Socolovsky M, Nam H, Fleming MD, Haase VH, Brugnara C, Lodish HF. Ineffective erythropoiesis in Stat5a(−/−)5b(−/−) mice due to decreased survival of early erythroblasts. *Blood.* 2001; 98(12):3261-3273.
36. Link A, Vogt TK, Favre S, et al. Fibroblastic reticular cells in lymph nodes regulate the homeostasis of naive T cells. *Nat Immunol.* 2007;8(11):1255-1265.
37. Webb JD, Coleman ML, Pugh CW. Hypoxia, hypoxia-inducible factors (HIF), HIF hydroxylases and oxygen sensing. *Cell Mol Life Sci.* 2009; 66(22):3539-3554.
38. Mahon PC, Hirota K, Semenza GL. FIH-1: a novel protein that interacts with HIF-1alpha and VHL to mediate repression of HIF-1 transcriptional activity. *Genes Dev.* 2001;15(20):2675-2686.
39. Kasper LH, Boussouar F, Boyd K, et al. Two transactivation mechanisms cooperate for the bulk of HIF-1-responsive gene expression. *EMBO J.* 2005;24(22):3846-3858.
40. McQuibban GA, Butler GS, Gong JH, et al. Matrix metalloproteinase activity inactivates the CXC chemokine stromal cell-derived factor-1. *J Biol Chem.* 2001;276(47):43503-43508.
41. Ceradini DJ, Kulkarni AR, Callaghan MJ, et al. Progenitor cell trafficking is regulated by hypoxic gradients through HIF-1 induction of SDF-1. *Nat Med.* 2004;10(8):858-864.
42. Forsythe JA. Activation of vascular endothelial growth factor gene transcription by hypoxia-inducible factor 1. *Mol Cell Biol.* 1996;16(9):4604-4613.
43. Simon MP, Tournaire R, Pouyssegur J. The angiopoietin-2 gene of endothelial cells is up-regulated in hypoxia by a HIF binding site located in its first intron and by the central factors GATA-2 and Ets-1. *J Cell Physiol.* 2008;217(3): 809-818.
44. Robey E, Chang D, Itano A, et al. An activated form of notch influences the choice between CD4 and CD8 T cell lineages. *Cell.* 1996;87(3):483-492.
45. Jin G, Zhang F, Chan KM, et al. MT1-MMP cleaves Dll1 to negatively regulate Notch signalling to maintain normal B-cell development. *EMBO J.* 2011;30:2281-2293.
46. Schmitt TM, Ciofani M, Petrie HT, Zuniga-Pflucker JC. Maintenance of T cell specification and differentiation requires recurrent notch receptor-ligand interactions. *J Exp Med.* 2004;200(4): 469-479.
47. Namen AE, Lupton S, Hjerrild K, et al. Stimulation of B-cell progenitors by cloned murine interleukin-7. *Nature.* 1988;333(6173):571-573.
48. Rolink A, Streb M, Nishikawa S, Melchers F. The c-kit-encoded tyrosine kinase regulates the proliferation of early pre-B cells. *Eur J Immunol.* 1991; 21(10):2609-2612.
49. Sudo T, Nishikawa S, Ohno N, Akiyama N, Tamakoshi M, Yoshida H. Expression and function of the interleukin 7 receptor in murine lymphocytes. *Proc Natl Acad Sci U S A.* 1993;90(19): 9125-9129.
50. Nagasawa T, Hirota S, Tachibana K, et al. Defects of B-cell lymphopoiesis and bone-marrow myelopoiesis in mice lacking the CXC chemokine PBSF/SDF-1. *Nature.* 1996;382(6592):635-638.

The American Journal of Pathology, Vol. 180, No. 6, June 2012
Copyright © 2012 American Society for Investigative Pathology.
Published by Elsevier Inc. All rights reserved.
http://dx.doi.org/10.1016/j.ajpath.2012.03.007

Stem Cells, Tissue Engineering, and Hematopoietic Elements

Generation of Kidney from Pluripotent Stem Cells via Blastocyst Complementation

Jo-ichi Usui,* Toshihiro Kobayashi,*† Tomoyuki Yamaguchi,*† A.S. Knisely,‡ Ryuichi Nishinakamura,§ and Hiromitsu Nakauchi*†

From the Division of Stem Cell Therapy, Center for Stem Cell Biology and Regenerative Medicine, Institute of Medical Science, University of Tokyo, Tokyo, Japan; the Japan Science Technology Agency,† ERATO, Nakauchi Stem Cell and Organ Regeneration Project, Tokyo, Japan; the Institute of Liver Studies,‡ King's College Hospital, London, United Kingdom; and the Department of Kidney Development,§ Institute of Molecular Embryology and Genetics, Kumamoto University, Kumamoto, Japan*

Because a shortage of donor organs has been a major obstacle to the expansion of organ transplantation programs, the generation of transplantable organs is among the ultimate goals of regenerative medicine. However, the complex cellular interactions among and within tissues that are required for organogenesis are difficult to recapitulate *in vitro*. As an alternative, we used blastocyst complementation to generate pluripotent stem cell (PSC)–derived donor organs *in vivo*. We hypothesized that if we injected PSCs into blastocysts obtained from mutant mice in which the development of a certain organ was precluded by genetic manipulation, thereby leaving a niche for organ development, the PSC-derived cells would developmentally compensate for the defect and form the missing organ. In our previous work, we showed proof-of-principle findings of pancreas generation by injection of PSCs into pancreas-deficient *Pdx1*$^{-/-}$ mouse blastocysts. In this study, we have extended this technique to kidney generation using *Sall1*$^{-/-}$ mouse blastocysts. As a result, the defective cells were totally replaced, and the kidneys were entirely formed by the injected mouse PSC-derived cells, except for structures not under the influence of *Sall1* expression (ie, collecting ducts and microvasculature). These findings indicate that blastocyst complementation can be extended to generate PSC-derived kidneys. This system may therefore provide novel insights into renal organogenesis. *(Am J Pathol 2012, 180:2417–2426; http://dx.doi.org/10.1016/j.ajpath.2012.03.007)*

At present, most patients with end-stage renal failure are treated by dialysis. Some patients eventually undergo kidney transplantation, but this option is limited by a shortage of donor organs. Therefore, the number of patients undergoing dialysis continues to grow, with complications, poor quality of life, and increasing medical costs. Moreover, the shortage of donor organs has led to other social problems, such as organ trafficking, transplant tourism, and transplant commercialism.[1] Under these circumstances, to transplant donor organs derived from pluripotent stem cells would be a much welcomed alternative. Induced-PSC (iPSC) technology[2,3] has recently enabled the generation of individual- or patient-derived PSCs, with studies of disease-targeting stem cell replacement therapy. However, the generation of an organ from iPSCs is considered impractical because it remains difficult to replicate *in vitro* the complex interactions among cells and tissues during organogenesis. To overcome this obstacle, we attempted to generate organs *in vivo* using the blastocyst complementation technique originally reported by Chen et al[4] in analyses of genes involved in lymphocyte development. We reported the successful application of this technique to generate PSC-derived mouse and rat pancreas in the *Pdx1*$^{-/-}$ mouse.[5] In the PSC-generated pancreas, defective cells were totally replaced, and the pancreas was formed almost entirely by the injected mouse and rat PSC-derived cells. The mouse and rat PSC-derived pancreas produced a variety of hormones, including insulin, and the transplantation of PSC-derived pancreas islets improved hyperglycemia in a diabetic mouse model. The premise driving this work is that a niche for organogenesis can be created in postblastocyst mutant mouse embryos that are genetically precluded from developing a particular or-

Supported by grants from the Japan Science Technology Agency (Ministry of Education, Culture, Sport, Science, and Technology, Japan).

Accepted for publication March 1, 2012.

J.U. and T.K. contributed equally to this work.

Current address of J.U., Department of Nephrology, Faculty of Medicine, University of Tsukuba, Tsukuba, Japan.

Address reprint requests to Hiromitsu Nakauchi, M.D., Ph.D., Division of Stem Cell Therapy, Center for Stem Cell Biology and Regenerative Medicine, Institute of Medical Science, University of Tokyo, 4-6-1 Shirokanedai, Minato-ku, Tokyo 108-8639, Japan. E-mail: nakauchi@ims.u-tokyo.ac.jp.

gan. Injected PSC-derived cells will colonize this developmental niche and compensate for the developmental defect to form a donor-induced organ *in vivo*.

Here we report our extended application of blastocyst complementation to generate kidneys from PSCs using *Sall1*$^{-/-}$ mice. *Sall1* is the mammalian orthologue of the Drosophila region-specific homeotic gene *spalt* (*sal*). Sall1 expression in the organism is restricted temporally to the period of nephrogenesis and disappears thereafter. Sall1 expression in the embryonic and newborn kidney is restricted histologically to metanephric mesenchyme and renal stroma. In embryonic kidney development, Sall1 is essential for ureteric bud attraction toward the mesenchyme. Mice deficient in *Sall1* therefore die soon after birth because of kidney agenesis or severe dysgenesis, whereas structures formed independently of *Sall1* such as the ureters and bladder are present.[6] This study was performed to establish whether *Sall1*$^{-/-}$ blastocysts offer a developmental niche for kidney tissue and could therefore be used to generate PSC-derived kidneys via blastocyst complementation.

Materials and Methods

Animals

C57BL6/NCrSlc, BDF1, and ICR mice were purchased from SLC Japan (Shizuoka, Japan). 129/OlaHsd (129/Ola) mice were purchased from Jackson Laboratory (Bar Harbor, ME). *Sall1* mutant-*EGFP* knock-in heterozygous mice were used for the production of ESC-derived chimeras[7] or *Sall1* knock-out heterozygous mice were used for the production of iPSC-derived chimeras.[6] They were crossed with C57BL/6 or BDF1 strain mice. In the *Sall1* mutant-EGFP knock-in heterozygous or homozygous mouse, EGFP fluorescence was limited to Sall1-expressing cells. All experiments were performed in accordance with the animal care and use guidelines of the Institute of Medical Science at the University of Tokyo.

Culture of Embryonic Stem Cells/iPSCs

Undifferentiated mouse embryonic stem cells (ESCs: EB3-DsRed) were maintained on gelatin-coated dishes without feeder cells in Glasgow's modified Eagle's medium (GMEM; Sigma-Aldrich, St. Louis, MO) supplemented with 10% fetal bovine serum (FBS; Nichirei Bioscience, Tokyo, Japan), 0.1 mmol/L 2-mercaptoethanol (Invitrogen, San Diego, CA), 0.1 mmol/L nonessential amino acids (Invitrogen), 1 mmol/L sodium pyruvate (Invitrogen), 1% L-Glutamine Penicillin Streptomycin (Sigma-Aldrich), and 1000 U/mL of leukemia inhibitory factor (LIF; Millipore, Bedford, MA). The EB3-DsRed cells, gifts from Dr. Hitoshi Niwa (CDB RIKEN), were derived from EB3 ES cells and carried the DsRed.T4 gene under the control of the CAG expression unit. The EB3 cells were a subline derived from E14tg2a ES cells[8] and were generated by targeted integration of the *Oct-3/4*-IRES-BSD-pA vector into the *Oct3/4* allele.[9]

Undifferentiated induced pluripotent stem cells (iPSCs: GT3.2) from mice were maintained on mitomycin-C–treated mouse embryonic fibroblast (MEF) cells in Dulbecco's modified Eagle's medium (DMEM; Invitrogen) supplemented with 15% knockout serum replacement (KSR; Invitrogen), 0.1 mmol/L 2-mercaptoethanol, 0.1 mmol/L nonessential amino acids, 1 mmol/L HEPES buffer solution (Invitrogen), 1% L-Glutamine Penicillin Streptomycin, and 1000 U/mL of LIF. The GT3.2 cells were generated from tail-tip fibroblasts of a male GFP transgenic mouse, kindly provided by Dr. Masaru Okabe (Osaka University) by the introduction of three factors (*Klf4*, *Sox2*, *Oct3/4*) in retroviral vectors. Viruses were prepared as described.[10] That GT3.2 cells ubiquitously express EGFP under the control of the CAG expression unit had been established.[5]

Embryo Manipulation

Preparation of *Sall1* heterozygous intercrossing embryos was performed as described.[11] In brief, eight cell/morula-stage embryos were collected in M2 medium (Millipore) from the oviducts and uteri of 2.5-day postcoital (dpc) *Sall1* heterozygous mice. These embryos were transferred into KSOM-AA medium (Millipore) droplets and cultured for 24 hours until development to the blastocyst stage.

For micromanipulation of the embryos, blastocysts were transferred into M2 medium droplets and the ESCs/iPSCs were trypsinized and suspended in the culture medium droplets. For each blastocyst, after careful drilling of the zona pellucida and trophectoderm under microscopy using a piezo-driven micromanipulator (Prime Tech, Tokyo, Japan), 10 to 15 ESCs/iPSCs were introduced into the blastocyst cavity near the inner cell mass. DsRed-marked ESCs were injected into blastocysts obtained by intercrossing of *Sall1*$^{+/EGFP}$ mice; EGFP-marked iPSCs were injected into blastocysts obtained by intercrossing of *Sall1*$^{+/-}$ mice. After injection, the embryos were cultured in KSOM-AA medium for 1 to 2 hours and were thereafter transferred into the uteri of 2.5-dpc pseudopregnant recipient ICR mice.

Flow Cytometry and Genotyping Analysis of ESC-Derived Chimeras

To identify the genotypes of neonatal *Sall1*-EGFP knock-in mice, EGFP-positive cells from the brain and kidney were sorted by fluorescence-activated cell sorting and genotyped by genomic PCR. The analysis and sorting were performed by Mo-flo (Beckman Coulter, Fullerton, CA) or using a FACS Vantage SE system (BD Bioscience Pharmingen, Franklin Lakes, NJ). DNA was extracted from collected cells using a QIAamp DNA Mini Kit (Qiagen, Germantown, MD) and was used to confirm mouse genotypes. The PCR primers used for the amplification of the wild-type *Sall1* allele and the mutated allele were as follows: 5′-AGCTAAAGCTGCCAGAGTGC-3′, 5′-CAACTTGCGATTGCCATAAA-3′, and 5′-GCGTTGGCTACCCGTGATAT-3′ (288 bp for the wild-type *Sall1* allele and 350 bp for the mutated allele).[7] Nested PCR primers were as follows: 5′-AGAATGTCGCCCGAGGTTG-3′, 5′-TACAGCAAGCTAGGAGCAC-3′, and 5′- AAGAGCTTGGCGGCGAATG-3′ (237 bp for the wild-type *Sall1* allele and 302 bp for the mutated allele). PCR amplification was performed as described elsewhere.[6,7]

Genotyping of iPSC-Derived Chimeras Using a Single EGFP-KSL Cell–Derived Colony or Splenocytes

To identify the genotypes of neonatal mice among the *Sall1* knock-out mice, single hematopoietic stem cells (HSCs) were assayed. Bone marrow cells were obtained from neonatal mice and suspended in PBS containing 3% FCS. Cells were stained with phycoerythrin (PE)–conjugated anti–Sca-1 monoclonal antibody (mAb; BD Bioscience Pharmingen), allophycocyanin (APC)–conjugated anti–c-Kit mAb, and a biotinylated anti-lineage antibody cocktail containing anti-Gr-1, anti–Mac-1, anti-B220, anti-CD4, anti-CD8, and anti-Ter-119 mAbs (e-Bioscience, Kyoto, Japan). The biotinylated antibodies were developed with APC-Cy7–conjugated streptavidin (SA: e-Bioscience). Single EGFP-negative KSL cells were collected in individual wells of round-bottomed, 96-well plates and cultured 10 to 14 days under conditions like those described,[5] but with one modification (erythropoietin was included in the culture medium instead of G-CSF, IL-6, and IL-11). EGFP-negative splenocytes were also prepared from the same mice and were collected by Mo-flo. DNA was extracted from colony-forming cells derived from single EGFP-KSL cells or splenocytes. The PCR primers used to amplify the neomycin-resistance (*neo*^{r}) gene inserted in the *Sall1* locus were: neo^r locus, forward 5′-AAGGGACTGGCTGCTATTGG-3′ and reverse 5′-ATATCACGGGTAGCCAACGC-3′ (420 bp); *Sall1* wild-type locus, forward 5′-GTACACGTTTCTCCTCAGGAC-3′ and reverse 5′- TCTCCAGTGTGAGTTCTCTCG-3′ (200 bp).[6] PCR amplification was performed as described above.

Histological Analysis

Kidneys were fixed with 4% paraformaldehyde and embedded in paraffin or, for frozen sections, in Optimal Cutting Temperature compound (Sakura Finetek, Japan). Paraffin sections were deparaffinized with xylene and hydrated with graded ethanols. A microwave oven was used for antigen retrieval. Paraffin sections were stained with hematoxylin and eosin (H&E) or periodic acid–methenamine silver (PAM) for light microscopy. Frozen sections were stained immunohistochemically. Briefly, each section was incubated with primary antibody overnight at 4°C and with secondary antibody for 1 hour at room temperature. Primary antibodies were anti-EGFP polyclonal antibody (pAb) for EGFP signal amplification (rabbit IgG, 1:500 dilution; Invitrogen), anti-DsRed pAb (rabbit IgG, 1:50 dilution; Clontech Laboratories, Mountain View, CA), anti-platelet endothelial cell adhesion molecule–1 (Pecam1) (mAb; rat IgG, 1:100 dilution; BD Bioscience Pharmingen), anti-aquaporin 1 (Aqp1) (pAb; rabbit IgG, 1:200 dilution; Chemicon International, Temecula, CA), anti-Liv2 (mAb; rat IgG, 1:200 dilution; Medical & Biological Laboratories, Nagoya, Japan), and anti-neuron class III β-tubulin (Tuj1) (mAb; rabbit IgG, 1:100 dilution; Covance, Emeryville, CA). Rhodamine- and biotin-labeled *Dolichos biflorus* agglutinin (DBA)–lectin, *Lotus tetragonolobus* (LT)–lectin, and peanut agglutinin (PNA)–lectin (Vector Laboratories, Burlingame, CA) staining was also performed. The secondary antibodies and fluorescence-conjugated streptavidin used for immunofluorescence studies were as follows: Alexa488-conjugated, Alexa546-conjugated, and Alexa647-conjugated goat anti-rabbit IgG (Invitrogen), Alexa546-conjugated and Alexa647-conjugated goat anti-rat IgG (Invitrogen), and Alexa546-conjugated and Alexa647-conjugated streptavidin (Invitrogen). After treatment with the appropriate antibodies, the sections were mounted with Vectashield mounting medium (Vector Laboratories) containing DAPI for nuclear staining and were observed by fluorescence microscopy or confocal laser scanning microscopy.

For ultrastructural analysis of glomeruli, chimeric kidneys were cut into tissue blocks (approximately 0.5 mm^3) and immersed in 2.5% phosphate-buffered glutaraldehyde overnight at 4°C. The tissue blocks were postfixed in 1% osmium tetroxide for 2 hours at 4°C, dehydrated in graded ethanols, and embedded in epoxy resin (Poly/Bed 812 Embedding Media, Polysciences, Warrington, PA). Ultra-thin sections cut on a Leica Ultracut S microtome (Leica, Vienna, Austria) were stained with uranyl acetate and lead citrate. Sections were observed by transmission electron microscopy (TEM) at 75kV using a H-7000 instrument (Hitachi, Tokyo, Japan).

Results

Generation of Kidney from Embryonic Stem Cells

We conducted blastocyst complementation using ESC and *Sall1*$^{EGFP/EGFP}$ blastocysts that would provide a niche for kidney development. As a result of blastocyst complementation (Figure 1, A and B), kidneys in *Sall1*$^{+/+}$ chimeric neonatal mice were red (data not shown). Kidneys in *Sall1*$^{+/EGFP}$ chimeric mice were yellow, reflecting a merger of host-derived EGFP-expressing cells and injected DsRed-marked ESC-derived cells, as in whole-body chimerism (*Sall1*$^{+/EGFP}$ in Figure 1B). On flow cytometry analysis, the brains and kidneys of *Sall1*$^{+/+}$ chimeric mice contained EGFP-negative and DsRed-expressing cells (Figure 2, C and D). The brains and kidneys of *Sall1*$^{+/EGFP}$ chimeric mice contained both EGFP-expressing and DsRed-negative cells and EGFP-negative and DsRed-expressing cells (Figure 2, E and F). The genotype of each fraction of sorted cells was confirmed by PCR (data not shown). The brains and kidneys of *Sall1*$^{+/EGFP}$ mice lacking ESC chimerism contained EGFP-expressing and DsRed-negative cells (Figure 2, A and B). The kidneys of *Sall1*$^{+/EGFP}$ mice intrinsically contained a few EGFP-expressing and DsRed-expressing cells (Figure 2B). In contrast, the kidneys of *Sall1*$^{EGFP/EGFP}$ chimeric neonatal mice were red throughout, indicating that the kidneys were entirely composed of DsRed-marked ESC-derived cells (*Sall1*$^{EGFP/EGFP}$ in Figure 1B), and were of normal size. The brains of *Sall1*$^{EGFP/EGFP}$ chimeric mice contained both EGFP-expressing and DsRed-negative

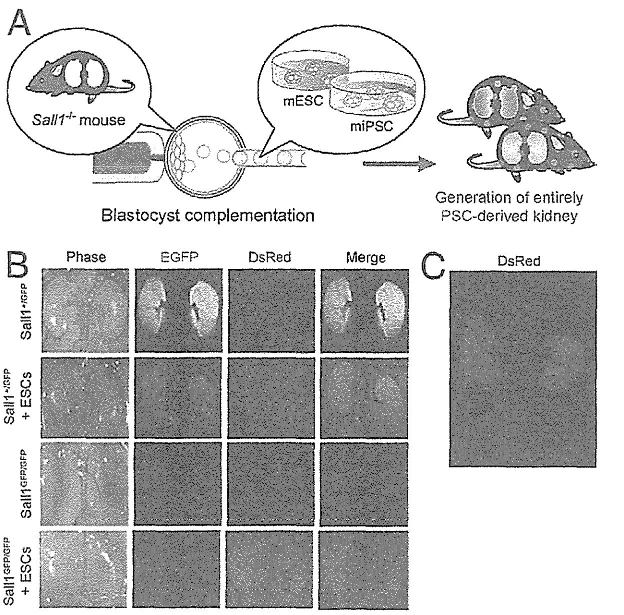

D

Injected cell	Parents	Analysis stage	Transferred embryos	No. of pups	No. of chimeras	Genotype +/+ or +/-	Genotype -/-
EB3-DR (ESC)	*Sall1*$^{+/EGFP}$ x*Sall1*$^{+/EGFP}$	Neonate	66	9	5	2	3
		Adult	79	34	24	24	0

Figure 1. ESC-derived kidneys generated by blastocyst complementation. **A:** Scheme for the experimental design for PSC-derived kidney generation. Embryos obtained from *Sall1* knock-out mice for kidney generation are injected with ESCs (EB3-DsRed) or iPSCs (GT3.2). Genotyping by PCR is performed; mice with entirely ESC- or iPSC-derived kidneys are generated. **B:** To identify kidneys clearly as being ESC derived or host derived, embryos obtained from intercrosses of *Sall1* EGFP knock-in mice (*Sall1*$^{+/EGFP}$) are injected with DsRed-marked ESCs. The kidneys of *Sall1*$^{EGFP/EGFP}$ mice complemented with ESCs are entirely positive for DsRed, indicating their ESC origin (*Sall1*$^{EGFP/EGFP}$ + ESCs in **B**). The kidneys of *Sall1*$^{+/EGFP}$ mice complemented with ESCs are positive for both DsRed and EGFP, indicating a mosaic of both ESC-derived and host-derived cells (*Sall1*$^{+/EGFP}$ + ESCs in **B**). **C:** Representative kidney almost entirely composed of DsRed-positive cells. **D:** Result of embryo manipulation and the genotype of *Sall1* mutant.

cells and EGFP-negative and DsRed-expressing cells (Figure 2G). By contrast, the kidney contained EGFP-negative and DsRed-expressing ESC-derived cells, but not EGFP-expressing and DsRed-negative host cells (Figure 2H). In ESC-derived *Sall1*$^{EGFP/EGFP}$ chimeric kidneys, host cells of collecting systems that did not express Sall1 were included in the EGFP-negative and DsRed-negative fraction (Figure 2H). These results indicate that ESC-derived kidney was formed in *Sall1*$^{EGFP/EGFP}$ mice by blastocyst complementation. A photograph of isolated kidneys, ureters, and bladder demonstrates the different densities of ESC-derived cells; although the kidneys were derived entirely from ESCs, the ESC contribution to ureters and bladder was minimal (Figure 1C). As expected, in both *Sall1*$^{EGFP/EGFP}$ and *Sall1*$^{+/EGFP}$ mice injected with DsRed-ESCs, ESC-derived cells contributed to all of the non-kidney tissues of the body, including adrenal gland, ureter, bladder, muscle, and adipose tissue (data not shown). The extent of the contribution varied from tissue to tissue and also from mouse to mouse depending on the individual degree of chimerism. Retrospective genotyping in a small population revealed that mice with *Sall1*$^{EGFP/EGFP}$, *Sall1*$^{+/EGFP}$, and *Sall1*$^{+/+}$ genotypes were born with Mendelian frequency (Figure 1D). These macroscopic and flow cytometry results substantiated that kidney had been formed in *Sall1*$^{EGFP/EGFP}$ mice via blastocyst complementation. However, no complemented mouse pup survived to adulthood (Figure 1D). By contrast, ESC-derived *Sall1*$^{+/EGFP}$ and *Sall1*$^{+/+}$ chimeric mice grew into adulthood (Figure 3, A and B). Moreover, ESC-derived *Sall1*$^{+/EGFP}$ chimeric mice and *Sall1*$^{+/+}$ chimeric mice were fertile (Figure 3C). An ESC-marking gene,

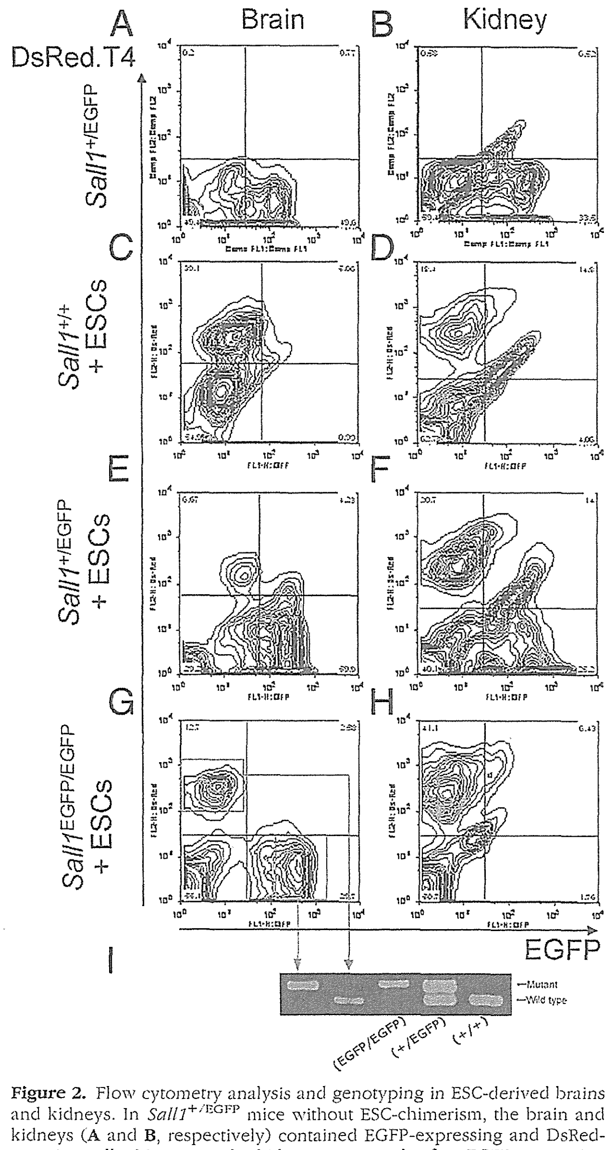

Figure 2. Flow cytometry analysis and genotyping in ESC-derived brains and kidneys. In *Sall1*$^{+/EGFP}$ mice without ESC-chimerism, the brain and kidneys (**A** and **B**, respectively) contained EGFP-expressing and DsRed-negative cells. Moreover, the kidneys contained a few EGFP-expressing and DsRed-expressing cells that showed autofluorescence. In *Sall1*$^{+/+}$ chimeric mice, the brain and kidneys (**C** and **D**, respectively) contained EGFP-negative &DsRed-expressing cells that were derived from ESCs. In *Sall1*$^{+/EGFP}$ chimeric mice, the brain and kidneys (**E** and **F**, respectively) contained both EGFP-expressing and DsRed-negative host cells and EGFP-negative and DsRed-expressing ESC-derived cells. **G:** In *Sall1*$^{EGFP/EGFP}$ chimeric mice, the brain contained both EGFP-expressing and DsRed-negative host cells and EGFP-negative and DsRed-expressing ESC-derived cells. **H:** Kidneys contained EGFP-negative and DsRed-expressing ESC-derived cells, but not EGFP-expressing and DsRed-negative cells. **I:** Genotyping PCR was performed on each fraction of sorted cells, as shown by boxed areas in **G**.

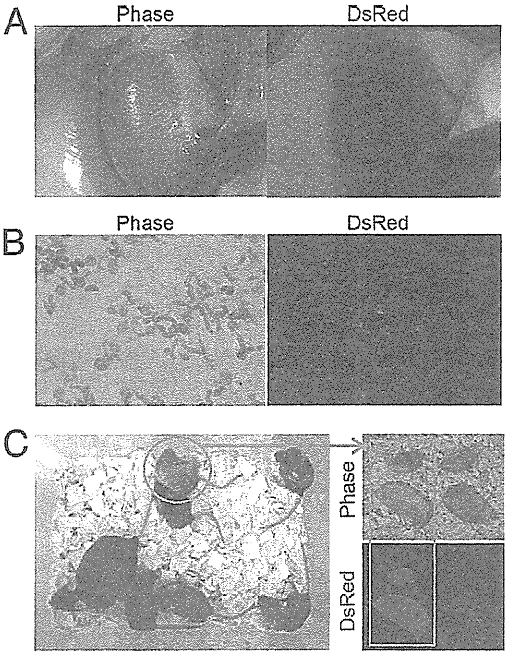

Figure 3. ESC-derived *Sall1*$^{+/EGFP}$ chimeric mice in adulthood. **A:** Kidney, muscle, and adipose tissue contained various contributions of ESC-derived cells. **B:** In ESC-derived chimeric kidneys fragmented with sieve mesh, some glomeruli and some tubules consisted of both ESC-derived cells and host-derived cells. **C:** ESC-derived *Sall1*$^{+/EGFP}$ chimeric mice were fertile. An ESC-marking gene, DsRed, was transmitted to progeny whose organs all exhibited DsRed fluorescence (**circle** in **left panel**, **square** in **right panel**).

DsRed, was transmitted to progeny whose organs all exhibited DsRed fluorescence. Figure 4 shows representative sections (H&E and PAM staining) of ESC-derived kidneys from pups of complemented *Sall1*$^{EGFP/EGFP}$ hosts. The glomerular capillary loops and basement membrane showed normal development, with blood cells in the glomerular capillary lumina (Figure 4, B and C). The glomerular podocytes and epithelium of Bowman's capsule were distinct, with open periglomerular urinary spaces (consistent with urine production). That is, the kidneys of these mice were grossly and histologically normal. Moreover, we examined these kidney tissues further for contributions of donor ESCs to different kidney lineages. On immunohistochemical study of kidneys of pups developed from embryos complemented with *Sall1*$^{EGFP/EGFP}$ blastomeres, the nephron epithelia (including the condensed mesenchyme, pretubular aggregate, comma-shaped bodies, s-shaped bodies, glomerular podocytes, Bowman's epithelia, proximal tubules, and distal tubules) and the renal stroma (including the cortical stroma and medullary stroma) consisted entirely of DsRed-positive cells (podocytes: Figure 4F; proximal tubules: Figure 4G; other data not shown). By contrast, both DsRed-positive cells and DsRed-negative cells were seen in collecting ducts (Figure 4H). Therefore, the tissues seen in this case were of ESC origin, with the exception of those in collecting-tubule epithelia. These data strongly indicate that we could generate ESC-derived kidneys by blastocyst complementation.

Generation of Kidney from iPSCs

We next addressed whether we could generate kidney from iPSCs instead of from ESCs. We used blastocysts derived from another *Sall1* knock-out mice, in which *EGFP* was not inserted, as injected iPSCs were marked with EGFP (Figure 1A). As expected, on macroscopy the kidneys of *Sall1*$^{+/-}$ or *Sall1*$^{+/+}$ chimeric mice were a mixture of host-derived cells and EGFP-marked iPSC-derived cells, as in whole-body chimerism (*Sall1*$^{+/-}$ in Figure 5A). In contrast, the kidneys of *Sall1*$^{-/-}$ chimeric mice were almost entirely composed of EGFP-marked iPSC-derived cells (*Sall1*$^{-/-}$ in Figure 5, A and B). These iPSC-derived kidneys of *Sall1*$^{-/-}$ chimeric mice were grossly normal in shape and size. As iPSC-derived kidneys had urine-filled bladders, those kidneys were inferred to communicate with ureters and to function well. In previous reports, the presence of bladders full of urine was shown to reflect functionality of the renal and urological systems in newborn mice.[6,12] Although we expect that the produced

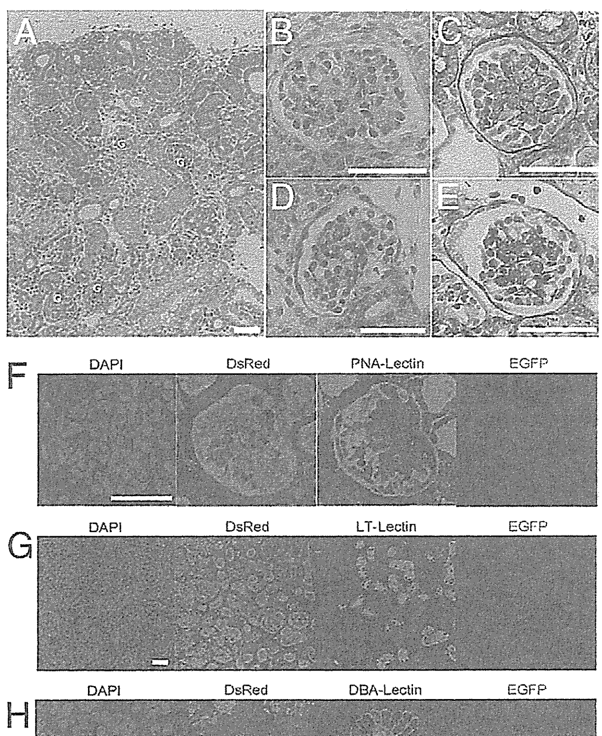

Figure 4. Histology and immunofluorescence of ESC-derived kidneys at the neonatal stage. **A:** Normal morphology in sections of kidney from *Sall1*$^{EGFP/EGFP}$ chimera. Mature glomeruli (G) were found. **B** and **C:** Glomeruli were normal in appearance in the *Sall1*$^{EGFP/EGFP}$ chimeric kidney. **D** and **E:** Glomerular features were normal in a wild-type 129/Ola strain from which ESCs had been established. H&E staining: **A, B,** and **D**; PAM staining: **C, E,** and **F–H:** Sections were stained with various lectins and anti-DsRed antibody; DAPI was used for nuclear counterstaining. **F:** PNA-lectin-positive glomerular podocytes were ¥ DsRed positive and EGFP negative. **G:** LT-lectin-positive proximal tubular epithelium was DsRed positive and EGFP negative. Most of the LT-lectin–negative tubular epithelia, including that of the distal tubules, were also DsRed-positive and EGFP-negative. **H:** DBA-lectin–positive collecting tubule epithelia were composed of both DsRed-positive ESC-derived cells and DsRed-negative host cells. Scale bar = 50 μm.

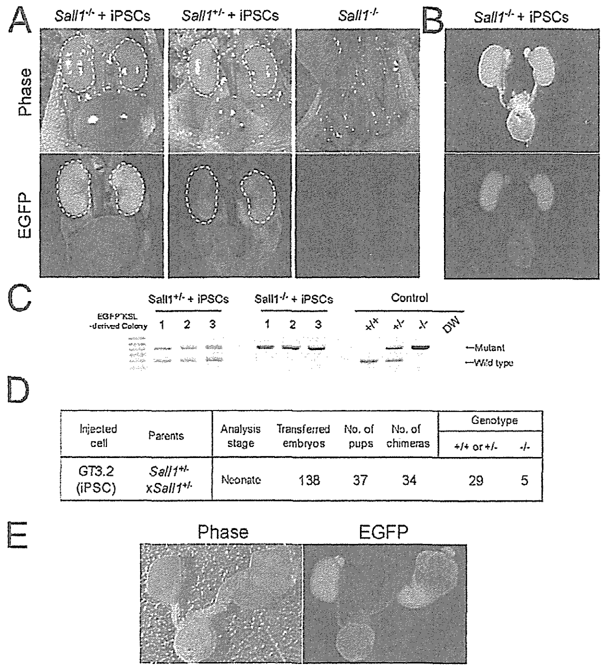

Injected cell	Parents	Analysis stage	Transferred embryos	No. of pups	No. of chimeras	Genotype	
						+/+ or +/-	-/-
GT3.2 (iPSC)	$Sall1^{+/-}$ x$Sall1^{+/-}$	Neonate	138	37	34	29	5

Figure 5. iPSC-derived kidneys generated by blastocyst complementation. **A:** iPSC-derived kidneys at the neonatal stage. In $Sall1^{-/-}$ mice complemented with iPSCs, the kidneys were normal in gross appearance and almost entirely positive for EGFP, indicating that they were of iPSC origin (**left panels**). The bladders of these mice were filled with urine. The kidneys in $Sall1^{+/-}$ mice complemented with iPSCs were only partially positive for EGFP, indicating the presence of a mosaic of both iPSC-derived and host-derived cells (**middle panels**). The absence of kidneys is shown in a non-chimeric $Sall1^{-/-}$ mouse at the same developmental stage (**right panels**). **B:** A representative kidney is almost entirely composed of EGFP-expressing cells. All of the non-kidney organs were mosaics of cells exhibiting fluorescence and of cells failing to fluoresce. **C:** Detection of *Sall1* mutant genotyping using genomic DNA extracted from colony-forming cells derived after single-cell sorting of EGFP-KSL cells from neonatal or postnatal bone marrow. **D:** Results of embryo manipulation and genotyping of *Sall1* mutant. **E:** In one $Sall1^{-/-}$ mouse complemented with iPSCs, the left kidney was hydronephrotic.

urine in newborns is more dilute than that in adults, we were unable to measure its osmolarity because of technical problems. As expected, in both $Sall1^{-/-}$ and $Sall1^{+/-}$ mice injected with EGFP-iPSCs, iPSC-derived cells contributed to all of the non-kidney tissues of the body, including adrenal gland, ureter, bladder, muscle, and adipose tissue (data not shown). The extent of the contribution varied from tissue to tissue and also from mouse to mouse depending on the individual degree of chimerism. Single HSC colony assays yielded material for genotyping PCR (Figure 5C). Retrospective genotyping revealed that mice with $Sall1^{+/+}$, $Sall1^{+/-}$, and $Sall1^{-/-}$ genotypes were born with Mendelian frequency (Figure 5D). In all $Sall1^{-/-}$ mice examined, regardless of donor chimerism in other tissues such as peripheral blood (range, 29.1% to 92%), kidneys formed bilaterally. In one mouse, one iPSC-derived kidney was normal and the other was hydronephrotic (Figure 5E). Whether this outcome was due to incomplete iPSC complementation or to other causes (eg, abnormally functioning iPSC-derived cells, $Sall1^{-/-}$ status) remains unclear. These gross findings suggest that iPSC-derived kidneys developed in $Sall1^{-/-}$ mice as a result of blastocyst complementation.

Next, we assessed histological findings in iPSC-derived kidneys. Figure 6 illustrates representative sections (H&E and PAM staining) of the kidney in pups of complemented $Sall1^{-/-}$ and $Sall1^{+/-}$ host blastocysts. On light microscopy of tissues from complemented $Sall1^{-/-}$ mice, like those from complemented $Sall1^{+/-}$ mice, the architecture of renal cortex and medulla was normal (Figure 6A). On immunofluorescence microscopy at low magnification, almost all tissues excluding DB-lectin–positive ureteric buds were EGFP positive. For signal amplification, we assessed the fluorescence of a chromophore coupled with anti-EGFP antibody. The glomerular capillary loops and basement membrane had formed normally, with blood cells in the glomerular capillary lumina (Figure 6B). The glomerular corpuscles were distinct, with open periglomerular urinary spaces consistent with urine production. On ultrastructural study, the glomerular three-layer architecture in complemented $Sall1^{-/-}$ mice was normal, with epithelial foot processes, basement membrane, and fenestrated capillary-loop endothelium (Figure 6C). At high magnification, slit diaphragms were seen (Figure 6D). The kidneys of these mice were grossly and histologically normal. These results clearly indicate that blastocyst complementation could generate both ESC- and iPSC-derived kidneys.

Polyclonal Origin of Single Glomerulus or Nephron in Mouse Chimeras

To buttress our conclusion that donor iPSCs contributed to different kidney lineages, we analyzed and compared immunohistochemical profiles. In this process, we incidentally confirmed a developmental phenomenon of chimeric mice. Immunohistochemical study of kidney in pups of $Sall1^{+/-}$ or $Sall1^{+/+}$ iPSC-derived chimeras found tissues of metanephric mesenchymal lineage, including glomerular podocytes in every glomerulus, to contain both EGFP-positive cells and EGFP-negative cells (Figure 6A, Figure 7A–D). Throughout nephrogenesis, the nephron progenitors and epithelia of metanephric mesenchymal lineage (ie, including the condensed mesenchyme, pretubular aggregate, comma-shaped bodies, s-shaped bodies, mature glomeruli, proximal and distal tubules) were similar. Among glomeruli, 28 had mixed EGFP-positive and EGFP-negative podocytes, two had only EGFP-positive podocytes, and one had only EGFP-negative podocytes. Moreover, other metanephric mesenchymal components (including the epithelia of Bowman's capsule and of the proximal and distal tubules) also showed a mixture of EGFP-expressing and non–EGFP-expressing cells (Figure 7D). In summary, individual metanephric mesenchymal components were composed of cells of polyclonal origin in mouse chimeras.

Immunohistochemical Analysis of iPSC-Derived Kidneys

We examined these kidney tissues further for contributions of donor iPSCs to different cell lineages. On immunohistochemical study of kidneys in pups from com-

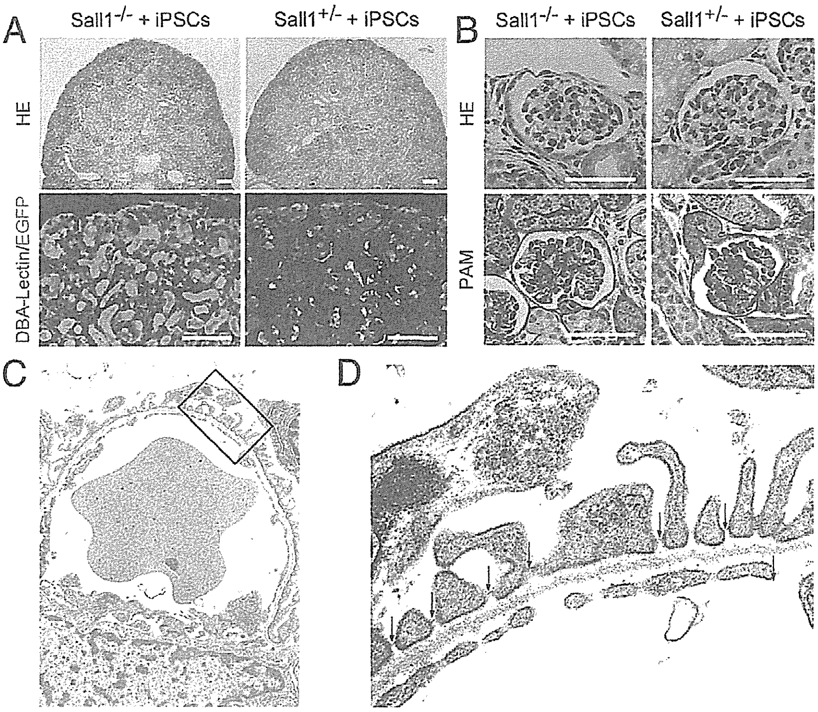

Figure 6. Histology of iPSC-derived kidneys at the neonatal stage. **A:** Normal morphology in sections of kidney from *Sall1*$^{-/-}$ chimera. Distribution of iPSC-derived cells in sections of iPSC-derived kidney from *Sall1*$^{-/-}$ and *Sall1*$^{+/-}$ hosts. **Upper panels:** Paraffin sections stained with H&E. **Lower panels:** Frozen sections stained for DBA-lectin and EGFP. Most of the nephron epithelia were of iPSC origin, but this was not the case for the DBA-lectin–positive ureteric bud epithelia. The cortical stroma was of iPSC origin (**asterisk**). Scale bar = 100 μm. **B:** Glomeruli were normal in appearance in *Sall1*$^{-/-}$ and *Sall1*$^{+/-}$ chimeric kidneys. Sections were stained with H&E or with PAM technique. Scale bar = 50 μm. **C:** Transmission electron micrograph of glomerulus in iPSC-derived kidney. The triple-layer architecture of the glomerular capillary in complemented *Sall1*$^{-/-}$ mice was normal, showing epithelial foot processes, basement membrane, and fenestrated capillary-loop endothelium. Original magnification, ×6000. **D:** High-power view of **boxed region** in **C**. Foot processes and slit diaphragms (**arrows**) exhibit normal development. Original magnification, ×20,000.

plemented *Sall1*$^{-/-}$ host blastocysts, the cells of metanephric mesenchymal lineage (including the condensed mesenchyme, pretubular aggregate, comma-shaped bodies, s-shaped bodies, mature glomeruli, proximal and distal tubules) were of iPSC origin, with the exception of the collecting duct epithelium (Figure 6A, Figure 7E–G). Most of the renal stroma (including the *cortical stroma, medullary stroma, and kidney capsule*) was of iPSC origin (Figure 6A, Figure 8A–C). This was to be expected, as the collecting ducts and ureters are originally derived from the ureteric bud; that is, development of these structures did not occur under the direct influence of *Sall1*.

The cortical stroma (A), in which nephron epithelia lie, medullary stroma (B), and Liv2-expressing kidney capsule (C) were replaced by EGFP-positive iPSC-derived cells. With respect to vascular systems, all of the endothelia of *vascular elements (including the arteries, arterioles, glo*merular endothelia, peritubular capillaries, and venules)

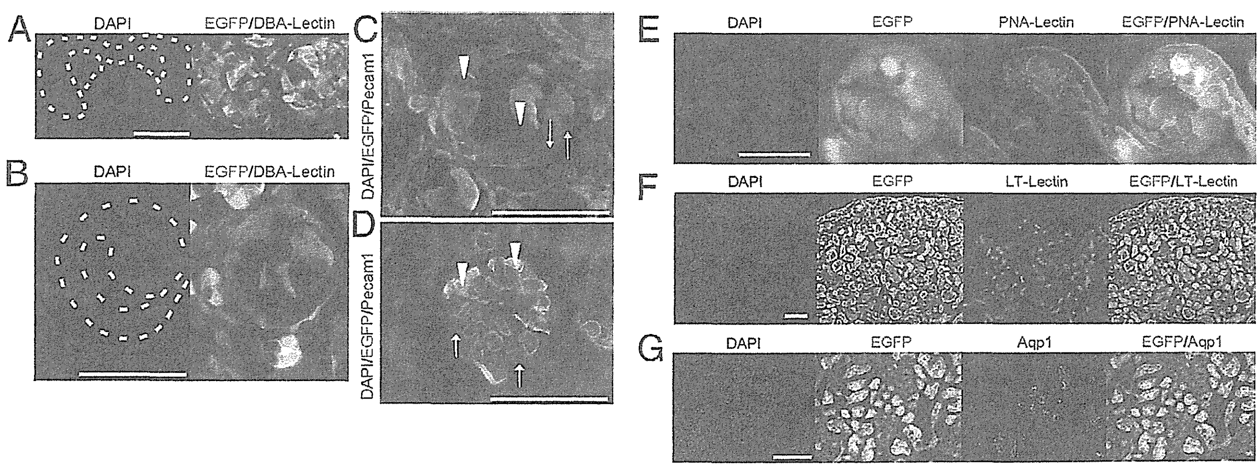

Figure 7. Immunofluorescence-microscopy studies of tissues of metanephric mesenchymal lineages in iPSC-derived kidneys at the neonatal stage. Polyclonal origin of a single glomerulus or tubule in mouse chimeras (using iPSC-derived kidney of *Sall1*$^{+/-}$ chimeras). **A** and **B:** Immunofluorescence in the iPSC-derived kidney of *Sall1*$^{+/-}$ chimeras. Metanephric mesenchymal lineages including condensed mesenchyme (**dashed line** in **A**), and comma-shaped bodies (**dashed line** in **B**) were mosaics of both iPSC- and host-derived cells. **C:** In the s-shaped body stage of the *Sall1*$^{+/-}$ chimeric kidney, a glomerular crevice with Pecam1-positive endothelial cells was seen. Presumptive glomerular podocytes (**white arrow**), Bowman's epithelia (**yellow arrow**), and the upper portion of the s-shaped body (**arrowhead**) were mosaics of both iPSC- and host-derived cells. **D:** In the mature glomerulus of *Sall1*$^{+/-}$ chimeric kidney, glomerular podocytes were hybrids of both EGFP-positive cells (**arrowheads**) and EGFP-negative cells (**arrows**). Scale bar = 50 μm. Immunofluorescence, iPSC-complemented *Sall1*$^{-/-}$ kidney (**E–G**). **E:** PNA-lectin–positive glomerular podocytes were totally composed of EGFP-positive iPSCs. **F:** LT-lectin–positive proximal tubular epithelia were of iPSC origin. **G:** In the medulla of the iPSC-complemented *Sall1*$^{-/-}$ kidney, tubular epithelia of Aqp1-positive thin limbs of loops of Henle were of iPSC origin. Scale bars: 50 μm (**A–D**); 25 μm (**E**); 100 μm (**F** and **G**).

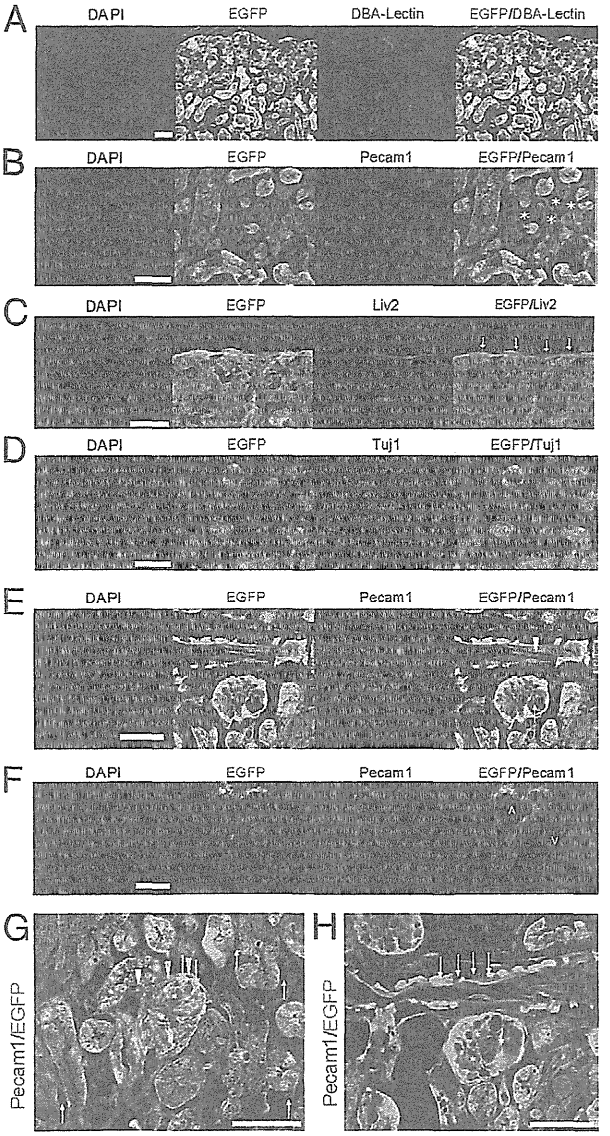

Figure 8. Immunofluorescence-microscopy studies of stromal components and vasculature in iPSC-complemented *Sall1*$^{-/-}$ kidneys at the neonatal stage. **A:** Most of the cortical stroma (**asterisk**) in which nephron epithelia lie was replaced by EGFP-positive iPSC-derived cells. **B:** The medullary stroma (**asterisk**) was of iPSC origin. **C:** Liv2-expressing kidney capsule, a layer of epithelial cells (**arrows**) cloaking the cortical surface, was of iPSC origin. **D:** Tuj1-expressing nerves around vessels in iPSC-derived kidney were not composed of iPSCs. **E:** Pecam1-expressing endothelium of glomerulus (**arrow**) and of interlobular artery (**arrowhead**) was chimeric, as shown by EGFP fluorescence. **F:** The Pecam1-expressing endothelium of segmental renal artery (A) and vein (V) was chimeric for EGFP. **G:** Pecam1-expressing endothelium of glomerulus, arteriole (**white arrowhead**), and peritubular capillary (**white arrows**) was chimeric for EGFP. Glomerular podocytes (**yellow arrows**) and Bowman's capsule epithelium (**yellow arrowheads**) were composed of EGFP-positive iPSC-derived cells. The glomerular mesangium (**asterisk**) was also of iPSC origin. **H:** In a section parallel to material shown in **E**, glomerular mesangium (**asterisk**) was of iPSC origin. Leiomyocytes (**arrows**) of interlobular artery were chimeric for EGFP. Scale bar = 50 μm.

showed chimeric organization (Figure 8E–H). The glomerular mesangium, but not the leiomyocytes of vessel walls, was of iPSC origin (Figure 8, G and H). In addition, nearly all juxtavascular or perivascular nerves were not of iPSC origin (Figure 8D). These results indicate that in all mice, although iPSCs supplied all kidney cell lineages, collecting duct epithelia and kidney stromal elements such as vessels and nerves were composites of host- and iPSC-derived cells.

Discussion

We have taken an innovative approach, that of blastocyst complementation, to organ regeneration and have demonstrated that this technique can be used to generate donor PSCs–derived functional kidney. If an empty developmental niche for an organ is provided (as with the *Pdx1*$^{-/-}$ mouse and the pancreatic niche[5]), PSCs-derived cellular progeny can occupy that niche and developmentally produce a solid organ in the vacant space. Several groups have used the same technique to study development of thymic epithelia[13] and compensation for cardiac defects,[14] to determine clonal origins in yolk sac hematopoiesis and germ cell development,[15,16] or to define developmental organ sizes of liver and pancreas.[17] Here, we applied this technique to the generation of kidneys.

Our present findings demonstrated that epithelial cellular lineages originating from the metanephric mesenchyme were entirely replaced by the progeny of injected PSCs in *Sall1*$^{-/-}$ chimeric mice (Figure 4, Figure 7). Sall1 is expressed in the metanephric mesenchyme–derived structures in the developing kidney, and is essential not only for the initial interactions between the mesenchyme and the ureteric buds but also for the growth and development of the metanephric mesenchyme after those interactions. Indeed, *in vitro* assays indicated that the Sall1-expressing cell population in the metanephric mesenchyme contains multipotent nephron progenitors, and that colony formation after plating was impaired in EGFP-positive cells from *Sall1*$^{EGFP/EGFP}$ mouse kidneys.[18] During nephrogenesis in the setting of blastocyst complementation, host embryo-derived cells in *Sall1*-deficient mice could not compete with injected normal ESC- or iPSC-derived cells. In addition, all renal stromal elements (ie, cortical stroma, medullary stroma, and kidney capsule) were composed of PSC-derived cells, suggesting that these tissues' development also depends on *Sall1* expression. It is worth noting that glomerular mesangial cells, but not leiomyocytes of vessel walls, were entirely composed of PSC-derived cells, although the cellular phenotype of mesangial cells reportedly resembles that of vascular leiomyocytes.[19] Our data therefore strongly indicate that *Sall1* exerts cell-autonomous functions in various lineages, including that of the metanephric mesenchyme, and that *Sall1* mutant mice could be useful as harboring a developmental niche in which to regenerate the major parts of the kidney by blastocyst complementation.

We consider that the mechanism for the rescue of tissues of renal stromal lineage including the renal capsule was related to cell-autonomous function during organ development. *Sall1* expression is reported not only in metanephric mesenchyme but also in *Foxd1*-expressing stromal components, although in the latter *Sall1* expression is relatively weak.[18] Our finding that the stroma is also replaced by PSC descendants may suggest that *Sall1* is also required for this lineage cell-autonomously, although lineage-specific *Sall1* deletion would be needed to test this hypothesis.

By contrast, collecting ducts derived from ureteric buds, microvascular endothelial cells including the glomerular endothelia, and leiomyocytes were not entirely composed of PSC-derived cells (Figure 8). These findings are consistent with the fact that *Sall1* is not expressed in the renal lineages mentioned above at kidney development. Therefore mutant mice lacking these lineages should be combined with *Sall1* knock-out mice if kidneys wholly composed of PSC descendants are to be generated.

In this study, none of the mouse pups with complemented kidneys survived to adulthood. Some chimeric mouse models with unexpectedly lethal phenotypes have been reported.[20,21] This suggests that chimerism does not always rescue mice from embryonic lethality, perhaps partly due to the insufficient multipotency of ESCs or to low proportional chimerism. *Sall1*$^{-/-}$ mice not only exhibited renal agenesis but also nursed poorly, as inferred from the absence of intragastric milk visible through the abdominal wall.[6] This was also true for blastocyst-complemented *Sall1*$^{-/-}$ pups. Because Sall1 is expressed in the brain, it may mediate the development of nerve pathways necessary for suckling function. Four *Sall* family genes were previously identified, *Sall1* to *Sall4*, and were demonstrated to act synergetically as transcription factors.[22,23] Therefore, each *Sall* family is possible to resemble in cellular function, and the phenotypes of the mutant mice may be similar each other. Among them, *Sall1* expression co-localizes with other *Sall* family expression, at sites such as the brain, kidney, limb buds, and heart. Indeed, *Sall3* mutant mice show anatomical defects in the brain,[24] permitting the inference that *Sall1*-deficient mice, without such defects, may have neurological functional abnormalities. Moreover, suckling ability can be adversely affected by other causes, including seeking the nipple, recognizing the nipple, orally grasping the nipple, sucking, and transport of oral contents to the back of the mouth, with swallowing. As expected, in PSC-injected *Sall1*$^{-/-}$ mice, both PSC-derived cells and host cells contributed to all non-kidney tissues. Therefore, neuromuscular and endocrine organs necessary for proper suckling were composites of both cell types, and physiological function may have been imperfectly recovered in these organs despite PSC-derived complementation. This perhaps illustrates an important aspect of blastocyst complementation, in that exogenous PSC-derived cells may not compensate for cell-intrinsic developmental defects that are not occasioned by cell loss. Alternatively, chimerism achieved by exogenous cells may not be sufficient to compensate fully for *Sall1* deficiency at some sites, and functional defects caused by *Sall1* deficiency may persist. Because of the lack of progression to adulthood, it was not possible to observe functioning of PSC-derived kidneys in adult mice. However, the observation of urine accumulation in the bladders of neonatal *Sall1*$^{-/-}$ mice derived from iPSC-complemented blastocysts strongly suggests that iPSC-derived kidneys were functional.

Previously we had successfully generated rat pancreas in mouse by injecting rat iPSCs into *Pdx1*$^{-/-}$ mouse embryos.[5] In this study, we also injected rat iPSCs into *Sall1*$^{-/-}$ mouse blastocysts; however, to date, we have not been able to generate rat kidneys in mice (unpublished observations). If the key molecules in mice involved in the interactions of the mesenchyme and the ureteric buds do not cross-react with those in rats, to vault this hurdle it would be necessary to generate a host mouse strain lacking all of the lineages that contribute to the kidney.

In summary, we successfully generated kidneys from PSCs via blastocyst complementation. This accomplishment may open doors to insights into the cellular and molecular mechanisms of kidney development.

Acknowledgments

We thank Satoshi Yamazaki, Sanae Hamanaka, Yuji Yamazaki, Yohei Morita, Hiroko Tsukui, and Tsutomu Kohda for their technical advice and Lin Franklin for critical review of the manuscript.

References

1. Summit SCotl: Organ trafficking and transplant tourism and commercialism: the Declaration of Istanbul. Lancet 2008, 372:5–6
2. Takahashi K, Yamanaka S: Induction of pluripotent stem cells from mouse embryonic and adult fibroblast cultures by defined factors. Cell 2006, 126:663–676
3. Takahashi K, Tanabe K, Ohnuki M, Narita M, Ichisaka T, Tomoda K, Yamanaka S: Induction of pluripotent stem cells from adult human fibroblasts by defined factors. Cell 2007, 131:861–872
4. Chen J, Lansford R, Stewart V, Young F, Alt FW: RAG-2-deficient blastocyst complementation: an assay of gene function in lymphocyte development. Proc Natl Acad Sci USA 1993, 90:4528–4532
5. Kobayashi T, Yamaguchi T, Hamanaka S, Kato-Itoh M, Yamazaki Y, Ibata M, Sato H, Lee YS, Usui J, Knisely AS, Hirabayashi M, Nakauchi H: Generation of rat pancreas in mouse by interspecific blastocyst injection of pluripotent stem cells. Cell 2010, 142:787–799
6. Nishinakamura R, Matsumoto Y, Nakao K, Nakamura K, Sato A, Copeland NG, Gilbert DJ, Jenkins NA, Scully S, Lacey DL, Katsuki M, Asashima M, Yokota T: Murine homolog of SALL1 is essential for ureteric bud invasion in kidney development. Development 2001, 128:3105–3115
7. Takasato M, Osafune K, Matsumoto Y, Kataoka Y, Yoshida N, Meguro H, Aburatani H, Asashima M, Nishinakamura R: Identification of kidney mesenchymal genes by a combination of microarray analysis and Sall1-GFP knockin mice. Mech Dev 2004, 121:547–557
8. Hooper M, Hardy K, Handyside A, Hunter S, Monk M: HPRT-deficient (Lesch-Nyhan) mouse embryos derived from germLine colonization by cultured cells. Nature 1987, 326:292–295
9. Niwa H, Miyazaki J, Smith AG: Quantitative expression of Oct-3/4 defines differentiation, dedifferentiation or self-renewal of ES cells. Nat Genet 2000, 24:372–376
10. Okabe M, Otsu M, Ahn DH, Kobayashi T, Morita Y, Wakiyama Y, Onodera M, Eto K, Ema H, Nakauchi H: Definitive proof for direct reprogramming of hematopoietic cells to pluripotency. Blood 2009, 114:1764–1767
11. Nagy A, Gertsenstein M, Vintersten K, Behringer R: Manipulating the mouse embryo: a laboratory manual. Cold Spring Harbor, NY, Cold Spring Harbor Laboratory Press, 2003
12. Hammes A, Guo JK, Lutsch G, Leheste JR, Landrock D, Ziegler U, Gubler MC, Schedl A: Two splice variants of the Wilms' tumor 1 gene

have distinct functions during sex determination and nephron formation. Cell 2001, 106:319–329
13. Muller SM, Terszowski G, Blum C, Haller C, Anquez V, Kuschert S, Carmeliet P, Augustin HG, Rodewald HR: Gene targeting of VEGF-A in thymus epithelium disrupts thymus blood vessel architecture. Proc Natl Acad Sci U S A 2005, 102:10587–10592
14. Fraidenraich D, Stillwell E, Romero E, Wilkes D, Manova K, Basson CT, Benezra R: Rescue of cardiac defects in id knockout embryos by injection of embryonic stem cells. Science 2004, 306:247–252
15. Ueno H, Weissman IL: Clonal analysis of mouse development reveals a polyclonal origin for yolk sac blood islands. Dev Cell 2006, 11:519–533
16. Ueno H, Turnbull BB, Weissman IL: Two-step oligoclonal development of male germ cells. Proc Natl Acad Sci USA 2009, 106:175–180
17. Stanger BZ, Tanaka AJ, Melton DA: Organ size is limited by the number of embryonic progenitor cells in the pancreas but not the liver. Nature 2007, 445:886–891
18. Osafune K, Takasato M, Kispert A, Asashima M, Nishinakamura R: Identification of multipotent progenitors in the embryonic mouse kidney by a novel colony-forming assay. Development 2006, 133:151–161
19. Lindahl P, Hellstrom M, Kalen M, Karlsson L, Pekny M, Pekna M, Soriano P, Betsholtz C: Paracrine PDGF-B/PDGF-Rbeta signaling controls mesangial cell development in kidney glomeruli. Development 1998, 125:3313–3322
20. Scacheri PC, Crabtree JS, Novotny EA, Garrett-Beal L, Chen A, Edgemon KA, Marx SJ, Spiegel AM, Chandrasekharappa SC, Collins FS: Bidirectional transcriptional activity of PGK-neomycin and unexpected embryonic lethality in heterozygote chimeric knockout mice. Genesis 2001, 30:259–263
21. He Y, Hakvoort TB, Vermeulen JL, Lamers WH, Van Roon MA: Glutamine synthetase is essential in early mouse embryogenesis, Dev Dynam 2007, 236:1865–1875
22. Sakaki-Yumoto M, Kobayashi C, Sato A, Fujimura S, Matsumoto Y, Takasato M, Kodama T, Aburatani H, Asashima M, Yoshida N, Nishinakamura R: The murine homolog of SALL4, a causative gene in Okihiro syndrome, is essential for embryonic stem cell proliferation, and cooperates with Sall1 in anorectal, heart, brain and kidney development. Development 2006, 133:3005–3013
23. Kawakami Y, Uchiyama Y, Rodriguez Esteban C, Inenaga T, Koyano-Nakagawa N, Kawakami H, Marti M, Kmita M, Monaghan-Nichols P, Nishinakamura R, Izpisua Belmonte JC: Sall genes regulate region-specific morphogenesis in the mouse limb by modulating Hox activities. Development 2009, 136:585–594
24. Parrish M, Ott T, Lance-Jones C, Schuetz G, Schwaeger-Nickolenko A, Monaghan AP: Loss of the Sall3 gene leads to palate deficiency, abnormalities in cranial nerves, and perinatal lethality. Mol Cell Biol 2004, 24:7102–7112

Distinct B-cell lineage commitment distinguishes adult bone marrow hematopoietic stem cells

Eliver Eid Bou Ghosn[a,1], Ryo Yamamoto[b], Sanae Hamanaka[b,c], Yang Yang[a], Leonard A. Herzenberg[a,1], Hiromitsu Nakauchi[b,c], and Leonore A. Herzenberg[a]

[a]Department of Genetics, Stanford University School of Medicine, Stanford, CA 94305; [b]Division of Stem Cell Therapy, Center for Stem Cell Biology and Regenerative Medicine, Institute of Medical Science, University of Tokyo, Tokyo 108-8639, Japan; and [c]Nakauchi Stem Cell and Organ Regeneration Project, Japan Science Technology Agency, Tokyo 108-8639, Japan

Contributed by Leonard A. Herzenberg, January 3, 2012 (sent for review December 5, 2011)

The question of whether a single hematopoietic stem cell (HSC) gives rise to all of the B-cell subsets [B-1a, B-1b, B-2, and marginal zone (MZ) B cells] in the mouse has been discussed for many years without resolution. Studies here finally demonstrate that individual HSCs sorted from adult bone marrow and transferred to lethally irradiated recipients clearly give rise to B-2, MZ B, and B-1b, but does not detectably reconstitute B-1a cells. These findings place B-2, MZ, and B-1b in a single adult developmental lineage and place B-1a in a separate lineage derived from HSCs that are rare or missing in adults. We discuss these findings with respect to known developmental heterogeneity in other HSC-derived lymphoid, myeloid, and erythroid lineages, and how HSC developmental heterogeneity conforms to the layered model of the evolution of the immune system that we proposed some years ago. In addition, of importance to contemporary medicine, we consider the implications that HSC developmental heterogeneity may have for selecting HSC sources for human transplantation.

The hematopoietic stem cell (HSC) derived from adult bone marrow (BM) is commonly thought to have multilineage potential, meaning that the HSC is considered capable of reconstituting all lymphoid, myeloid, and erythroid lineages of the immune system (1, 2). Indeed, HSCs from BM readily replenish B, T, myeloid, and erythroid cells in irradiated recipients (3, 4). However, more detailed examination of the reconstituted B cells derived from HSCs taken at different times during development reveals differences in reconstitution efficiency for the four currently recognized murine B-cell subsets, [i.e., B-1a, B-1b, B-2, and marginal zone B (MZ)] (5–7).

Transferring adult BM into lethally irradiated recipients readily reconstitutes B-2 and MZ, which represent the majority of the B cells in spleen and other lymphoid organs but only poorly reconstitute B-1 cells in the same recipients. In contrast, transferring neonatal BM, liver, or spleen to similar irradiated recipients fully reconstitutes B-1 (B-1a and B-1b), B-2, and MZ. Thus, at least with respect to B cells, the multilineage potential of the HSC population in adults is more limited than the multilineage potential of the HSC population in neonates (5, 7–12). These differences in B-cell reconstitution capabilities of adult versus neonatal BM underlie the idea that B-1 and B-2 belong to distinct developmental lineages derived from distinct HSCs (13).

Recent studies by Dorshkind and colleagues (5) confirm and extend the earlier findings. By sorting and transferring highly enriched HSC populations from adult BM and neonatal sources, these investigators demonstrate that the HSC population sorted from adult BM principally reconstitutes B-2 and B-1b and only poorly reconstitutes B-1a (5). In contrast, B-1a cells are relatively well reconstituted by transfers of HSC populations sorted from "neonatal" BM (2.5 wk of age), although the sorted cells still predominantly reconstitute B-2 and B-1b (5). These findings demonstrate clearly that the commitment to give rise to develop into B-1a occurs at or before the HSC development and that BM HSC populations collectively lose the potential to give rise to B-1a as the animal ages.

Importantly, however, because the Dorshkind studies are based on transfers of sorted HSC populations (roughly 1,000 sorted cells per recipient), they are not informative with respect to the potential of individual HSCs in the transferred population to give rise to each of the B-cell subsets (B-1a, B-1b, B-2, and MZ). In studies here, we close this gap by definitively demonstrating that individual HSCs sorted from adult BM fully reconstitute B-2, MZ, and some B-1b but do not reconstitute B-1a. These findings place B-2, MZ, and at least some B-1b in a single adult developmental lineage and place B-1a in a separate lineage derived from HSCs that are rare or missing in adults.

We discuss these findings with respect to known developmental heterogeneity in other HSC-derived lymphoid and myeloid lineages in the mouse (14, 15) and how/whether HSC developmental heterogeneity conforms to the layered model of the evolution of the immune system that we proposed some years ago (13, 16). In addition, of importance to contemporary medicine, we consider the implications HSC developmental heterogeneity for selecting HSC sources for human transplantation.

Results

Adult Bone Marrow Transfers Poorly Reconstitute B-1a in Irradiated Recipients. Multiple studies show that B-1 cells, which represent the majority of the B cells in the peritoneal cavity (PerC), are only poorly reconstituted by adult bone marrow transfers that readily reconstitute B-2 cells in the PerC and elsewhere in irradiated recipients (7, 8, 10–12). However, B-1 are readily reconstituted by transfers of mature B-1 from adult PerC to the same irradiated recipients. Similarly, we show here that B-1 are poorly reconstituted by transfers of 3×10^6 adult BALB/c (IgH^a allotype) BM cells to sublethally irradiated (3.25 Gy) $RAG1^{-/-}$ recipient mice (Fig. 1). Cotransfer of 3×10^6 adult PerC cells from CB.17 (IgH^b allotype) congenic mice reconstitutes only B-1 in the same animals (Fig. 1).

At the B-cell subset level, adult BM (IgH^a) transfers reconstitute B-2 and a small percentage of B-1b ($CD5^-$ B-1) but only very few B-1a ($CD5^+$ B-1). The extent of this minimal B-1a and B-1b reconstitution decreases with the number of BM cells transferred, more so for B-1a than B-1b (Table 1). Thus, B-1a reconstitution falls below detectability at 2×10^5 transferred BM cells, whereas this number of transferred BM still reconstitutes B-1b ($CD5^-$ B-1) to a reasonable extent (Table 1). These findings are consistent with distinctive origins for B-1a and B-2 and raise questions about the developmental relationship between B-1a and B-1b. Studies that follow address these issues.

Author contributions: E.E.B.G., Leonard A. Herzenberg, H.N., and Leonore A. Herzenberg designed research; E.E.B.G. and R.Y. performed research; R.Y. and S.H. contributed new reagents/analytic tools; E.E.B.G., Y.Y., Leonard A. Herzenberg, H.N., and Leonore A. Herzenberg analyzed data; and E.E.B.G. and Leonore A. Herzenberg wrote the paper.

The authors declare no conflict of interest.

[1]To whom correspondence may be addressed. E-mail: eliverg@stanford.edu or lenherz@darwin.stanford.edu.

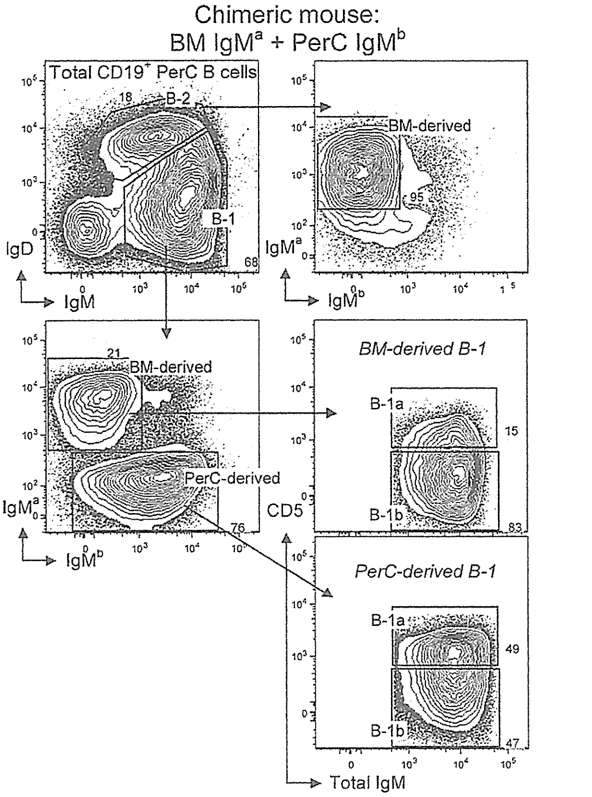

Fig. 1. Reconstitution of recipient peritoneal cavity (PerC) B cells after cotransfer of bulk bone marrow (BM) and PerC. Donor cells (3×10^6 BALB/c BM and 3×10^6 CB.17 PerC) were injected i.v. to sublethally irradiated RAG1$^{-/-}$ recipients. Two months after transfer, B-cell reconstitution was analyzed in recipient PerC as shown. Donor BM (IgM^a) cells readily reconstituted B-2 (IgD^{hi}, IgM^{lo}) and B-1b (IgD^{lo}, IgM^{hi}, CD5$^-$) in PerC of recipient mice. In contrast, donor PerC (IgM^b) cells mainly reconstituted B-1a (IgD^{lo}, IgM^{hi}, and CD5$^+$) and B-1b.

Single HSCs Sorted from Adult BM and Transferred to Lethally Irradiated Recipients Provide Long-Term Reconstitution of All Hematopoietic Cells. For these studies, we FACS sorted and transferred a *single* HSC obtained from adult BM of transgenic mice expressing Kusabira Orange (KuO$^+$), a readily detectable fluorescent marker, and identified as Lin$^-$ cells that express c-Kit$^+$, Sca-1$^+$, CD150$^+$ but not CD34 (17) (Fig. 2*A*). Each individual HSC was transferred i.v. to lethally irradiated mice along with 2×10^5 "competitor" congenic BM cells. Mice were bled monthly to check for the level of chimerism, i.e., percentage of immune cells derived from the single HSC (KuO$^+$) versus percentage of immune cells derived from the competitor congenic BM. Preliminary analysis demonstrated significant hematopoietic

Table 1. The extent of B-1 (B-1a and B-1b) reconstitution changes with the number of donor bone marrow (BM) transfers

	PerC B-1 cells derived from donor BM cells, %	
Amount of donor BM	B-1a	B-1b
3×10^6 total cells	12–20	80–88
2×10^5 total cells	2–5	95–98
Single HSC	0.2–1	99–99.8

B-1a (CD5$^+$ B-1) reconstitution falls below detectability at 2×10^5 transferred BM cells, whereas B-1b (CD5$^-$ B-1) are still reasonably reconstituted.

reconstitution (i.e., multilineage reconstitution) in 17/80 recipients of sorted HSC. Here, we examined the five recipients that had the highest chimerism in the B-cell compartment (10–80% of total B cells in blood derived from sorted KuO$^+$ HSCs).

Despite the difference in its ability to reconstitute B-1a versus B-2 (*Results*), the individually transferred HSCs studied here were fully multipotent, at least by the current definition of multipotency, i.e., they stably reconstituted platelets, erythrocytes, myeloid cells, T cells, and B cells in all recipient mice. These reconstituted hematopoietic cells were still readily detectable when the mice were killed and the organs harvested at 30 wk posttransfer.

Individual HSCs Sorted from Adult BM Give Rise to B-2 and B-1b, but Not to B-1a: Reconstitution in Recipient PerC. Transfers of individual HSCs to irradiated recipients are well known to reconstitute B-2 cells, which typically predominate in spleen and peripheral blood and are commonly taken as a measure of B-cell reconstitution (4). We similarly find that B-2 cells are readily reconstituted by transfers of single HSCs from adult bone marrow to irradiated recipients and that B-1b are reconstituted to about half-normal level (Fig. 2*B*). However, even 30 wk after transplantation, individual HSCs sorted and transferred from adult bone marrow do not replenish the B-1a compartment in the otherwise fully reconstituted recipients (Fig. 2*B*).

This selective B-1a developmental failure cannot be explained by a lack of support for B-1a development in the adult recipient environment. Earlier transfer studies have clearly shown that B-1a cells are readily reconstituted when early progenitors (fetal liver, neonatal spleen, and BM) are transferred to adult recipients (11). Moreover, Dorshkind et al. (5) have shown directly that bulk-sorted and transferred neonatal HSCs readily reconstitute B-1a cells in adult recipients. These and other similar findings demonstrate clearly that the adult environment readily supports development of B-1a. Therefore, the failure of the HSCs in our study to give rise to B-1a demonstrates that adult BM contains HSCs that are restricted developmentally to giving rise only to B-2 and some B-1b.

Of course, adult BM may also contain HSCs capable of giving rise to all B-cell subsets, including B-1a. Indeed, Dorshkind and colleagues obtained some B-1a reconstitution when they transferred 500–1,000 sorted HSCs from adult BM to irradiated recipients (5). In any event, because we failed to obtain B-1a in 5/5 HSC recipients, the data we present here (Fig. 2*B*) clearly demonstrate that a sizable proportion of HSCs in adult BM cannot reconstitute B-1a.

Surprisingly, given the close historical and notational relationship between B-1a and B-1b (9, 11), we find that all of the individually sorted and transferred adult HSCs replenish a substantial proportion of the B-1b compartment (Fig. 2*B*). Thus, we additionally conclude that adult HSCs are committed to give rise to B-2 and a proportion of B-1b cells.

Individual HSCs Sorted from Adult BM Give Rise to Follicular (B-2) and MZ B Cells, but Not B-1a: Reconstitution in Recipient Spleen. Consistent with data for PerC reconstitutions presented above, individually sorted adult BM-derived HSCs do not reconstitute detectable numbers of B-1a cells (B220^{lo}, CD5$^+$) in spleen (Fig. 3). As expected, these HSCs efficiently reconstitute splenic follicular B-2 (IgD^{hi} and IgM^{lo}) cells and MZ (CD21^{hi}) B cells. Moreover, the percentage of CD21^{hi} MZ cells among total B cells derived from the sorted HSCs is similar to that found in the spleen of control animals.

Discussion

We have shown that individual HSCs, FACS sorted from adult BM and transferred to lethally irradiated recipients, give rise to B-2, MZ B, and B-1b cells but do not give rise to B-1a. These

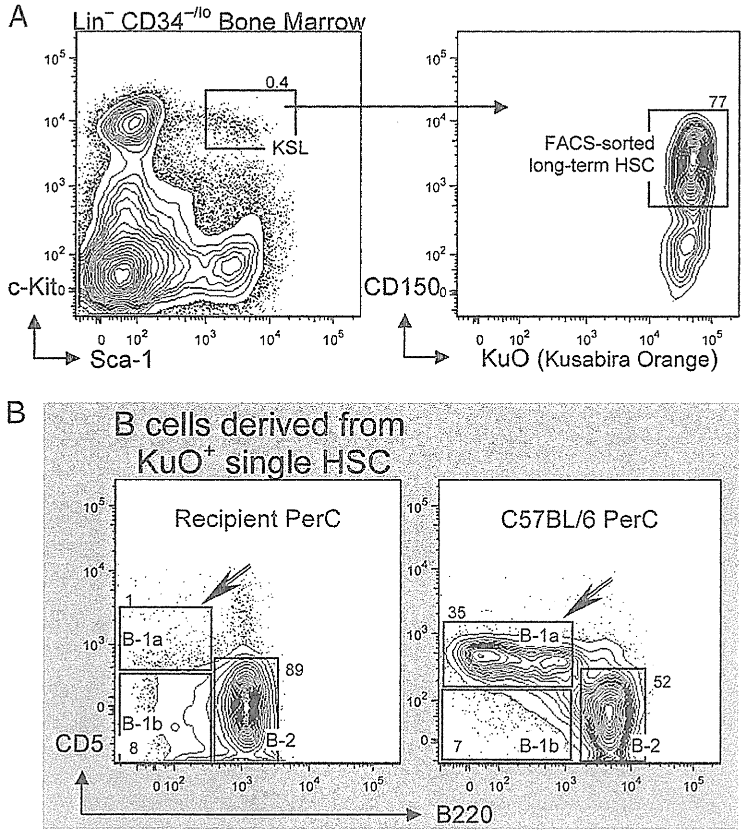

Fig. 2. Reconstitution of recipient peritoneal cavity (PerC) B cells after single HSC transfer. Individual HSCs were isolated from adult (9 wk) bone marrow (BM) of KuO$^+$ mice and injected i.v. to lethally irradiated C57BL/6 recipients. (*A*) HSC in adult BM was identified as Lin$^-$, c-Kit$^+$, Sca-1$^+$, CD150$^+$, and CD34$^{-/lo}$. (*B*) Recipient PerC was analyzed 27 wk after single HSC (KuO$^+$) transfer. Total HSC-derived B cells in recipient PerC were identified by CD19$^+$ and KuO$^+$ and analyzed for surface expression level of CD5 and B220. Sorted and transferred individual KuO$^+$ HSC failed to reconstitute B-1a (CD5$^+$, B220^{lo}, and CD19^{hi}) but readily reconstituted B-2 (CD5$^-$, B220^{hi}, and CD19^{lo}) and some B-1b (CD5$^-$, B220^{lo}, and CD19^{hi}).

findings confirm the longstanding hypothesis that B-1a and B-2 originate from distinct progenitors in adults and hence belong to distinct developmental lineages (6, 7, 10, 11, 18–24). Further, these findings unexpectedly place a proportion of B-1b and MZ in the same developmental lineage as B-2.

Laying the groundwork for these findings, Dorshkind et al. (5) have shown that 500–1,000 bulk-sorted HSCs from adult BM principally reconstitute B-2 in lethally irradiated recipients. In addition, small but detectable numbers of B-1a (roughly 6% of total B in PerC) were reconstituted by the 500–1,000 bulk-sorted BM cells that were transferred (5). In our studies, transfers of individual HSCs also fully reconstituted B-2. However, these transfers failed to detectably reconstitute B-1a (only a few scattered "dots" constituting at best 0.2–1% of total B in PerC were visible in FACS analyses) (Figs. 2*B* and 3). The difference can be explained if rare HSCs capable of giving rise to B-1a were present in the HSC bulk sorted from adult BM in the previous study.

Dorshkind et al. have already shown that B-1a are clearly, albeit not fully, reconstituted by HSC bulk sorted from 2.5-wk-old neonatal BM (5). Thus, it is reasonable to expect that a small number of neonatal HSCs are present among sorted adult HSC populations. These HSCs could either reconstitute both B-1a and B-2 (plus MZ and B-1b) or they could be committed to reconstitute only B-1a. There is no data at present to decide between these alternatives. In any event, the current data collectively demonstrate that a high proportion (most or all) adult HSCs are committed to reconstitute only B-2, MZ, and some B-1b.

Fetal liver and neonatal (2 d–2 wk) spleen, of course, have long been known to fully reconstitute B-1 and all other B-cell subsets in irradiated recipients (11). As in intact animals, the number of B-1a is greater than B-2 and B-1b (B-1a > B-2 > B-1b) in PerC in these recipients. In contrast, B-2 > B-1b > B-1a in PerC in recipients of the HSC populations sorted and transferred from 2.5 wk BM, although B-1a reconstitution by the sorted neonatal cells is still substantially greater than B-1a reconstituted from HSC bulk sorted from adult BM (5). Thus, either HSCs gradually lose their ability to reconstitute B-1a as animals age or the HSCs in adults never had this ability, i.e., they are developmentally distinct from the HSCs that predominate during fetal and neonatal life (6, 13, 21). Again, there are no data available to distinguish these possibilities. See Table 2 for a comprehensive description of B-cell reconstitution potential of several in vivo cell transfer studies (2, 5, 11, 22–26).

In any event, the differences in B-cell development potential between neonatal and adult HSCs indicate that evolution has crafted a developmental strategy for differentially populating the B-cell compartment to gradually enrich it for functionally relevant B cells as the animal ages (13, 16). This strategy would appear to extend to all hematopoietic lineages in the mouse. Differences between fetal and adult erythrocytes are well known. Further, early work from the Weissman and Allison laboratories defined a "first wave" of T-cell development, which occurs during fetal life and principally generates $\gamma\delta$ T cells and later wave(s) that generate the $\alpha\beta$ T cells that ultimately predominate in adult life (27). In this construction, B-1a would be located alongside $\gamma\delta$